Perturbation Analysis and Simulation Study of the Effects of Phase on the Classical Hydrogen Atom Interacting with Circularly Polarized Electromagnetic Radiation

Daniel C. Cole and Yi Zou

Dept. of Manufacturing Engineering, 15 St. Mary's Street,

Boston University, Brookline, Massachusetts 02446

(Dated: October 28, 2003)

Abstract

The classical hydrogen atom is examined for the situation where a circularly polarized electromagnetic plane wave acts on a classical charged point particle in a near-circular orbit about an infinitely massive nucleus, with the plane wave normally incident to the plane of the orbit. The effect of the phase α of the polarized wave in relation to the velocity vector of the classical electron is examined in detail by carrying out a perturbation analysis and then comparing results using simulation methods. By expanding the variational parts of the radius and angular velocity about their average values, simpler nonlinear differential equations of motion are obtained that still retain the key features of oscillating amplitude, namely, the gradual increase of the envelope of the oscillating amplitude and the point of rapid orbital decay. Also, as shown here, these key features carry over nicely to conventional quantities of interest such as energy and angular momentum. The phase α is shown here to have both subtle yet very significant effects on the quasistability of the orbital motion. A far wider range of phase conditions are found to provide stability than might intuitively be expected, with the time to orbital decay, t_d, varying by orders of magnitude for any plane wave with an amplitude A above a critical value, A_c.

keywords: hydrogen, Rydberg, stochastic, electrodynamics, simulation classical, nonlinear

I. INTRODUCTION

The present article continues the study of the classical hydrogen atom system interacting with radiation, as reported in Refs. [1] and [2]. Somewhat surprisingly, there has apparently been little detailed simulation work regarding a classical charged point particle orbiting an infinitely massive and oppositely charged classical nucleus when this system is acted upon by a variety of types of classical electromagnetic radiation. Initially, of course, around 1900, this was the main physical picture that physicists had of the simplest of atomic systems (hydrogen). However, the apparent obvious result of the decay of the orbit, in a time frame of about 1.3×10^{-11} sec, appeared to have dissuaded most scientists from taking this physical picture too seriously, since it seemed obvious to most that such a simple physical picture could not possibly provide a close physical description of nature. Bohr's initial quantized model of the atom, involving selected orbits that would not radiated, then led scientists to develop the description of nature we call quantum mechanics.

Nevertheless, there are a number of reasons for reexamining this simple classical system. The study of Rydberg atoms, both theoretically and experimentally, has been quite fruitful for scientific investigations in recent years [3], [4], [5], [6], [7], [8]. To aid in understanding the rich and complex phenomena observed in these relatively simple Rydberg systems, often semiclassical physical ideas are used. However, to date, these semiclassical ideas have either entirely, or largely, ignored the effects of radiation reaction, and have only been concerned with the general Keplerian type orbits, without the perturbed effects of radiation reaction. We expect the present research direction to aid in furthering such physical reasoning and to help improve semiclassical modeling of such atomic systems.

Second, we expect that a close analysis of the classical electrodynamic hydrogen atom, when acted upon by rapid and strong electromagnetic fields, should enable further advances in controlling such simple systems. Engineers and scientists have in recent years been suggesting a variety of possible applications of such ideas, ranging from "storing information" in Rydberg-like systems [9], to better controlling chemical reactions [10],[11], as well as manipulating and utilizing plasma etching systems and sources for ion implantation. Some of these systems are so very complicated, that simulation of them seems essential to help guide the possible experiments and physical understanding.

Third, clearly from the mathematical perspective regarding nonlinear systems and chaotic

theory, this relatively simple classical system is far from being understood in any depth. Moreover, there are underlying symmetries [12], [13], [14] that should strongly influence its behavior; only the beginnings of such studies have been carried out to date.

Lastly, the classical exploration of this simplest of atomic physical systems, aided by simulation methods, may shed further insight on the relevancy of a proposed theory of nature called stochastic electrodynamics (SED). This theory was developed by a number of researchers, with major developments by Marshall [15],[16] and Boyer [17],[18] in the 1960s, that proposed that quantum phenomena was a result of the natural interaction of classical charged particles with classical electromagnetic radiation. A key element of the SED physical ideas was that a classical hydrogen atom must be in thermodynamic equilibrium with classical electromagnetic radiation, if it is to result in any sort of stable-like behavior. Boyer in Ref. [19] appears to have been the first to clarify and investigate the ideas here for hydrogen (also see Refs. [20] and [21]). If a classical electron orbits a classical nucleus, then of course it must radiate electromagnetic radiation. However, if a classical system of charged particles is to have any hope of being in a thermodynamic equilibrium state, then on average as much energy radiated off must be equal to the work done by radiation on the charged particles. The qualitative SED picture arises that the classical electron orbits the classical nucleus, always radiating off electromagnetic energy, sometimes faster, and sometimes slower, depending on it's instantaneous rapidity of movement. Likewise, the thermal radiation acting on the electron does work on the particle, sometimes positive work, and sometimes negative work, and of different magnitudes at different times. On average, though, it does just as much net positive work as is radiated off by the electron during its stochastic motion, in large part because of the natural correlation of motion that arises between the motion of the electron and the thermal radiation; *i.e.*, if they are to be in thermodynamic equilibrium, then of course, there must be a correlation, of fundamental significance, between the fluctuations of the thermal radiation and the atomic systems embedded in the radiation bath.

As first discussed in Ref. [19], the qualitative idea behind this correlative motion is the following: the closer the particle is to the nucleus, the smaller the period of its motion about the nucleus and the more likely it is to have positive work done on it by the higher frequency components of the thermal radiation, thereby on average acting to increase the orbit of the particle. Likewise, the larger the radius of the particle from the nucleus, the larger the

period of the effective orbit and the more the lower frequency components of the radiation will be the dominant part of the radiation that acts on the orbit. However, since the average amplitude of the radiation of these lower frequency components is smaller, then the average effect is not sufficient to offset the energy always being radiated by the particle's motion, and the average effect is to have the orbit decrease. In this way, a stochastic-like motion should arise, resulting in the radius decreasing and increasing, but in such a way to agree with the stability observed in nature. Related points are discussed further in other work, such as Refs. [22], [23], and [24].

Although few scientists are familiar with these notions, a number of researchers have deeply probed the possibilities of this theory. Many ideas that seemed impossible to explain by classical physics alone, were shown to be at least partly explainable from this stochastic-like interaction between classical electromagnetic fields and classical charged particles [19], [24], [23]. However, deeper quantitative probing revealed difficulties with these ideas, particularly when the hydrogen atom was examined in close detail [25], [26], [**?**], [27]. Boyer [12] and Cole [13] suggested that the problem with these approaches might be the difficult nonlinear equations involved in real physical, Coulombic based systems in nature. However, to date, improvements in solving these equations of motion have not been obtained, possibly because of the difficulty in carrying out the full analysis, combined undoubtedly with the doubt that most physicists have of the likelihood of success of this research program.

However, Refs. [1] and [2] showed that the simple classical electrodynamic model of hydrogen, even without the full thermodynamic radiation spectrum acting, already reveals fascinating nonlinear behaviors that at the very least beg for further understanding at a mathematical level, but may also reveal deep physical insights that could help to propel the investigations of SED forward yet again. The aim of the present article is to continue this investigation on the next logical level, namely, more deeply understanding the nonlinear behavior and interaction of particle movement and applied fields. Indeed, our preliminary numerical experiments to date indicate that the richness and surprisingly complex behavior of this simplest of atomic systems [28] has only begun to be uncovered in terms of such classical analysis [29]. The recent work reported in Refs. [29] and [30] provide further evidence that, indeed, the ideas of SED may well hold for hydrogen, with Ref. [30] reporting on the results of numerical simulations that show surprisingly close results from SED to the

quantum mechanical ground state probability distribution function for hydrogen.

We now turn to a brief summary of the work in Refs. [1] and [2], where it was shown that a classical charged point particle, obeying the Lorentz-Dirac equation of motion [31], while under the interaction of a Coulombic binding potential and sets of classical electromagnetic plane waves, can maintain stable patterns of motion under a far wider range of conditions than might normally be expected. Reference [1] began this work by studying near-circular motion and showing that circularly polarized (CP) plane waves near the same orbital frequency of the classical electron's orbit, can greatly influence the behavior of the orbit. When the amplitude of the CP plane wave is above a particular value, the electron's orbit will slowly spiral out and in for relatively long periods of time, before eventually becoming out of step with the CP wave and then decaying in orbit.

Reference [2] continued this analysis to the more general, but more difficult, situation of elliptical orbits. For this case, a spectrum of CP waves was required to achieve the same orbital balance, where the detailed spectral shape was a function of the eccentricity, ε, of the orbit ($\varepsilon = 0$ means a circular orbit, while $\varepsilon \to 1$ entails a highly eccentric one). As shown, the more eccentric the orbit, the more important become the higher frequency harmonics associated with the period of the orbit. If the amplitudes of the CP plane waves that balanced the near elliptical orbit were scaled linearly above their critical balance point, then it was found that a similar behavior to the circular case resulted, where the semimajor and semiminor axes would spiral out and in, over and over again, until eventually orbital decay would begin. The values of the periodicity and the amplitude of this spiraling motion, for both the circular and elliptical cases, were found to be highly dependent on the scaling factor of the CP waves that balanced the orbit.

In the present article, a deeper study of this nonlinear behavior will be carried out. Since much of the physical aspects is contained in the much simpler, near-circular orbital situation, this is what we will concentrate on here. We begin in Sec. II by examining in detail the situation of a near-circular, spiralling orbit as discussed in Ref. [1], but now showing how the same patterns for the radius also carry over to the energy, angular momentum, and other important physical factors. In Sec. III, a perturbation analysis is carried out to help reveal the important factors of this pattern of stability and decay. As shown here, some very subtle and nonintuitive effects occur regarding stability via the simple change of altering the phase of the incident CP plane wave in relation to the velocity of the orbiting electron. A

far wider range of phases than might otherwise be expected is shown to provide quasi-stable behavior, with the time to decay being very significantly altered by this simple change in phase. Indeed, as will be shown in a subsequent article, for any CP, normally incident plane wave, with an amplitude falling within a very wide range of values that will be clarified later, an *infinite* time of stability can be achieved, by properly selecting the phase and angular frequency of the CP wave. We should qualify this claim by emphasizing that this result holds in the nonrelativistic approximation treated here. However, it appears that most of this work will carry over nicely, but of course with differences, to where the problem is treated fully relativistically.

Finally, Sec. IV ends with a few concluding remarks summarizing the results found here. The perturbation analysis helps us to better understand some of the key characteristics of the nonlinear behavior of this simple classical atomic system. We note, that much of the analysis in the present article forms a direct natural basis for the work reported in Ref. [29].

II. STABILITY AND DECAY, MONITORED BY ENERGY AND ANGULAR MOMENTUM

As shown in [1], if a classical electron with charge $-e$ and rest mass m orbits a classical nucleus with charge $+e$ and assumed infinite mass (this can be readily corrected, but does not influence our main points here), then the classical radiation reaction will result in the orbit steadily decaying in radius. However, if the classical electron starts out in a circular orbit of radius a, and is acted upon by a CP plane wave traveling in a direction normal to the plane of the orbit, with the phase and amplitude of the CP wave carefully chosen as discussed in Ref. [1], then the radiation reaction can be precisely balanced so that the orbit does not decay. To achieve this balance, the electric field amplitude of the CP wave needs to equal, in the nonrelativistic approximation,

$$A_c \equiv \frac{2e^3\omega_c}{3mc^3a^2} = (\omega_c\tau)\,\frac{e}{a^2} \quad , \tag{1}$$

where $\tau \equiv \frac{2e^2}{3mc^3}$ and the angular frequency of the orbit and of the CP plane wave is

$$\omega_c \equiv \left(\frac{e^2}{ma^3}\right)^{1/2} \quad . \tag{2}$$

(The subscript "c" on A_c stands for "critical", in the sense of the smallest incident amplitude that allows stability; the associated angular velocity ω_c ensures a circular orbit at radius a.)

Most of Ref. [1] was devoted to examining what happens when $A > A_c$. The general behavior can be quickly understood by looking at a particular example. Figure 1 shows a situation where the initial circular orbit is 0.5 Å, the CP wave is initially out of phase by $\pi/4$ with the electron's motion, and $A = 100$ statvolt, which is about 18.5 times larger than the value of $A_c = 5.419$ statvolt needed to maintain a perfect circular orbit of radius $a = 0.5$ Å. As can be seen, the orbit steadily spirals in and out about $r = 0.5$ Å. As shown in Fig. 1(b), the envelope of the r vs. t curve gradually increases, until finally decay sets in, as shown in the blown up version in Fig. 1(c) near $t = 3.227 \times 10^{-12}$ sec. Much of Ref. [1] described why these effects occur, from the point of view of the positive versus negative work done by the CP plane wave on the orbiting particle, during its spiraling in and out motion. In the next section, we will analyze these properties much more deeply.

However, before proceeding with this task, it seems of some interest to observe how the general trends shown in Fig. 1 for r versus t, translate into other properties of the particle's motion during this same time period, such as for energy, $E = \frac{1}{2}m\mathbf{v}^2 - \frac{e^2}{r}$, and angular momentum, $\mathbf{L} = \mathbf{r}\times(m\mathbf{v}) = \hat{\mathbf{z}}m\,(x\dot{y} - y\dot{x})$. After all, one might suspect that if other quantities were tracked, such as the usual "conserved" quantities of energy and angular momentum, then a deeper insight might be revealed of the dynamics of this behavior. However, as seen in Fig. 2, the basic behavior of these quantities behaves very similar in character to the radius variations in Fig. 1. Although we did not make a duplicate blown-up version of Fig. 1(b) for the energy and angular momentum, this property also of the envelope gradually increasing until decay sets in, holds for these two variables as well. A similar behavior holds for a variety of other quantities, such as speed versus time. (Note that in Figs. 2(c) and 2(d), $L_z < 0$; if $|L_z|$ was plotted, then the magnitude would decrease after the transition point.)

The reason for the variation in energy and angular momentum of the orbiting classical electron is that these quantities are not conserved; the CP plane wave does both positive and negative work on the electron, increasing and decreasing its energy. If we plot the total force in the tangential direction of the motion, acting on the electron, including the radiation reaction, this force varies very systematically between about -5.06×10^{-8} and $+4.54 \times 10^{-8}$ dynes throughout the entire range of time shown in Fig. 1(a); however, its character changes significantly at the point when orbital decay sets in, as illustrated in Fig. 3(a). If we superimpose the energy and tangential force curves, as in Fig. 3(b), then it can

be seen that the peaks and valleys of the energy curve coincide perfectly with the points where the tangential force equals zero.

Of course, energy and angular momentum in the global sense are conserved. If one considers a volume enclosing the orbit of the electron, then the change in the sum of kinetic energy plus electromagnetic energy of all the sources of electromagnetic fields precisely equals the electromagnetic energy that flows into this volume within any given interval of time. Alternatively, the work done in a given time period by the CP plane wave on the classical electron is precisely equal to the change in the kinetic plus electromagnetic energy associated with the electron and classical nucleus, minus the electromagnetic energy that flows out of this volume due to these two electromagnetic sources. A similar statement holds for the angular momentum. References [23] and [32] provide further details on these statements.

Clearly, a key point to the pattern of the continued spiraling in and out motion, eventually leading to the point of decay, has to do with the relation of the electron's angular position, θ, about the classical nucleus, versus the net "angle", ωt, of the CP plane wave. Eventually they become too much "out of step", and decay sets in. Precisely how this occurs will be the focus of the next section. Figure 4 shows the relationship of $\theta - \omega t$ versus t, where $x = r\cos(\theta)$ and $y = r\sin(\theta)$. As can be seen in Figs. 4(a) and 4(b), $(\theta - \omega t)$ falls within a tight range between about -4.7 to $+0.64$, or about -1.5π to 0.20π, all the way until the transition point, at which point θ and ωt become greatly out of step. Figure 4(b) shows the characteristic feature of the envelope curve widening, while Fig. 4(c) shows the region near the transition point. As can be seen there, the top peak of each of the maxima to the left of the decay point become increasingly more and more flat the closer to the point of decay. This is a key feature that will be brought out more fully in a later publication involving a deeper analysis of the decay time of these orbits.

III. PERTURBATION ANALYSIS OF MOTION

We will now turn to a perturbation analysis of the orbiting particle's motion in an attempt to probe the essential features of the nonlinear behavior examined in earlier plots. Our treatment here will be nonrelativistic (NR), with plans to cover much of the relativistic treatments in a future publication. We will treat the electron as being confined to the $x-y$ plane, with the particle traveling in a counterclockwise direction, starting at $x = a$, $y = 0$.

We will assume the plane wave propagates in the $-\hat{\mathbf{z}}$ direction with angular frequency ω and electric field amplitude A, with the electric field in the $x-y$ plane given by

$$\mathbf{E}_{\rm CP} = A\left[\hat{\mathbf{x}}\cos\left(\omega t - \frac{\pi}{2} + \alpha\right) - \hat{\mathbf{y}}\cos\left(\omega t + \alpha\right)\right] \quad . \tag{3}$$

The value of α allows us to adjust the phase of the CP wave to make the electron's orbital decay sooner or later (see Fig. 9 in Ref. [1]); for the simulation in Fig. 1, $\alpha = -\pi/4$. The NR equations of motion for the x and y coordinates of the orbiting particle then become

$$m\ddot{x} = -\frac{e^2 x}{|\mathbf{z}|^3} - eA\cos\left(\omega t - \frac{\pi}{2} + \alpha\right) - \frac{2e^4}{3mc^3}\left(\frac{\dot{x}}{|\mathbf{z}|^3} - \frac{3x\left(x\dot{x}+y\dot{y}\right)}{|\mathbf{z}|^5}\right) \ , \tag{4}$$

and

$$m\ddot{y} = -\frac{e^2 y}{|\mathbf{z}|^3} + eA\cos\left(\omega t + \alpha\right) - \frac{2e^4}{3mc^3}\left(\frac{\dot{y}}{|\mathbf{z}|^3} - \frac{3y\left(x\dot{x}+y\dot{y}\right)}{|\mathbf{z}|^5}\right) \quad . \tag{5}$$

The last terms in Eqs. (4) and (5) represent the NR approximation of the radiation reaction $\mathbf{R}_{\rm reac}$ in the Lorentz-Dirac equation [31], where

$$\mathbf{R}_{\rm reac} \approx \frac{2e^2}{3c^3}\dddot{\mathbf{z}} \approx \frac{2e^2}{3c^3}\frac{d}{dt}\left\{\frac{-e^2\mathbf{z}}{|\mathbf{z}|^3 m}\right\} = -\frac{2e^4}{3mc^3}\left[\frac{\frac{d\mathbf{z}}{dt}}{|\mathbf{z}|^3} - \frac{3\mathbf{z}(\mathbf{z}\cdot\frac{d\mathbf{z}}{dt})}{|\mathbf{z}|^5}\right] \quad . \tag{6}$$

Here we have ignored the contribution to the radiation reaction due to the contribution of the plane wave, since the force it exerts in the simulations we are investigating here is so very much smaller than the binding Coulombic force of the classical nucleus. We have verified that if the latter contribution was included, the effect would not be noticeable in the simulation results we show here. (*I.e.,* nearly all figures shown here would be altered unperceptively.) The only real change of signficance might be on our examination of "infinite time without decay", as including this term would alter that analysis. However, the length of time to decay would still be enormously long. We prefer to include the contribution of this "plane wave" contribution to the radiation reaction in later work when we report on a full relativistic analysis, as the size of this additional term is so very small, and since our NR radiation reaction term of $\frac{2e^2}{3c^3}\dddot{\mathbf{z}}$ is already an approximation of the term in the full Lorentz-Dirac equation. Thus, to clarify, the "nonrelativistic" results we are reporting here, hold for the case of Eqs. (4) and (5), with the approximation made in Eq. (6) for the radiation reaction.

A perturbation analysis of Eqs. (4) and (5) can be carried out by noting that the radius of the particle undergoes a small oscillatory perturbation up until the point of orbital decay.

In contrast, the angular position θ, minus ωt, is not a small number, as it varies on the order of magnitude of $\pm\pi$ until the point of decay. However, the angular velocity $\dot{\theta}$, does only vary by a small amount from ω, up until this point. Hence, we will write:

$$x(t) = [a + \delta(t)]\cos(\theta) \quad , \tag{7}$$

and

$$y(t) = [a + \delta(t)]\sin(\theta) \quad , \tag{8}$$

where we will assume that $|\delta| \ll a$ up until the point of orbital decay, where a is the initial radius. Also, we will assume that

$$\dot{\theta} = \omega + \dot{\phi} \quad , \tag{9}$$

where $\left|\dot{\phi}\right| \ll \omega$.

We next expand each of the quantities in Eq. (4) to first order in the terms δ/a and its derivatives, and $\dot{\phi}$ and its derivatives. (The following treatment applies equally to Eq. (5), but does not provide any additional information.) Hence:

$$\dot{x} \approx -a\omega\sin(\theta) + a\left[-\dot{\phi}\sin(\theta) + \frac{\dot{\delta}}{a}\cos(\theta) - \frac{\delta}{a}\omega\sin(\theta)\right] \quad , \tag{10}$$

$$\begin{aligned}\ddot{x} &\approx -a\omega^2\cos(\theta) \\ &+ a\left[-\ddot{\phi}\sin\theta - 2\omega\dot{\phi}\cos\theta + \frac{\ddot{\delta}}{a}\cos\theta - 2\frac{\dot{\delta}}{a}\omega\sin\theta - \frac{\delta}{a}\omega^2\cos\theta\right] \quad ,\end{aligned} \tag{11}$$

$$\dot{y} \approx a\omega\cos(\theta) + a\left[\dot{\phi}\cos(\theta) + \frac{\dot{\delta}}{a}\sin(\theta) + \frac{\delta}{a}\omega\cos(\theta)\right] \quad , \tag{12}$$

$$-\frac{e^2 x}{|\mathbf{z}|^3} \approx -\frac{e^2\cos(\theta)}{a^2} + \frac{2e^2\cos(\theta)}{a^2}\frac{\delta}{a} \quad , \tag{13}$$

$$\begin{aligned}&-\frac{2e^4}{3mc^3}\left(\frac{\dot{x}}{|\mathbf{z}|^3} - \frac{3x\,(x\dot{x} + y\dot{y})}{|\mathbf{z}|^5}\right) \\ &\approx \frac{2e^4\omega\sin\theta}{3mc^3a^2} + \frac{2e^4}{3a^2mc^3}\left(+\dot{\phi}\sin\theta + 2\frac{\dot{\delta}}{a}\cos\theta - 2\frac{\delta}{a}\omega\sin\theta\right) \quad .\end{aligned} \tag{14}$$

Substituting these quantities into Eq. (4) and requiring that $\omega = \omega_c$,which would be the angular frequency of the orbiting particle in a circular orbit if the radiation reaction and effects of the plane wave could be ignored, then we obtain

$$\begin{aligned} & am\left[-\ddot{\phi}\sin(\theta) - 2\omega\dot{\phi}\cos(\theta) + \frac{\ddot{\delta}}{a}\cos(\theta) - 2\frac{\dot{\delta}}{a}\omega\sin(\theta) - \frac{\delta}{a}\omega^2\cos(\theta)\right] \\ & = \frac{\delta}{a}\frac{2e^2\cos(\theta)}{a^2} - eA\sin(\omega t+\alpha) + \frac{2e^4\omega\sin(\theta)}{3mc^3a^2} \\ & \quad + \frac{2e^4}{3a^2mc^3}\left[\dot{\phi}\sin(\theta) + 2\frac{\dot{\delta}}{a}\cos(\theta) - 2\frac{\delta}{a}\omega\sin(\theta)\right] \quad . \end{aligned} \tag{15}$$

The above result agrees with the finding in Ref. [1] that when $\theta = \omega t + \alpha$, $\delta = 0$, $\dot{\phi} = 0$, and all higher derivatives of δ and $\dot{\phi}$ equal zero, then the amplitude of the CP electric field is given by Eq. (1). This relationship comes from the two terms $\left[-eA\sin(\omega t+\alpha) + \frac{2e^4\omega\sin(\theta)}{3mc^3a^2}\right]$ on the right side in Eq. (15). Physically, what is happening is that the force from the plane wave is balancing the radiation reaction term. It should be noted that these two terms depend rather weakly on $\dot{\phi}$ (in the term $\sin(\theta) = \sin\left[\omega t + \int dt\dot{\phi}\right]$), and they do not depend directly on δ. However, if $A > A_c$, then $-eA\sin(\omega t+\alpha) + \frac{2e^4\omega\sin(\theta)}{3mc^3a^2}$ on the right side of Eq. (15) should serve as sort of a forcing function for the rest of the terms.

By substituting

$$\sin(\omega t+\alpha) = \sin[\theta(t) - \phi(t) + \alpha] = \sin(\theta)\cos(\phi-\alpha) - \cos(\theta)\sin(\phi-\alpha) \tag{16}$$

into Eq. (15), and requiring that the equation holds for all values of θ, thereby equating coefficients of $\cos(\theta)$ and $\sin(\theta)$, we obtain:

$$+\left[\ddot{\phi} + \omega^2\tau\dot{\phi} - \frac{eA}{am}\cos(\phi-\alpha) + \tau\omega^3\right] + \left[2\omega\frac{\dot{\delta}}{a} - 2\tau\omega^3\frac{\delta}{a}\right] = 0 \quad , \tag{17}$$

$$-\left[2\omega\dot{\phi} + \frac{eA}{am}\sin(\phi-\alpha)\right] + \left[\frac{\ddot{\delta}}{a} - 2\omega^2\tau\frac{\dot{\delta}}{a} - 3\omega^2\frac{\delta}{a}\right] = 0 \quad , \tag{18}$$

where $\tau = \frac{2e^2}{3mc^3}$ and Eq. (2) were used to simplify the expressions.

We carried out simulations, numerically solving Eqs. (17) and (18) for the range of conditions in Ref. [1]. For later comparisons, we will refer to the solutions of Eqs. (17) and (18) as being "case P1". These solutions were obtained by substituting $w_1 \equiv \frac{\delta}{a}$, $w_2 \equiv \frac{\dot{\delta}}{a}$, $w_3 \equiv \phi$, and $w_4 \equiv \dot{\phi}$, into Eqs. (17) and (18), resulting in four first-order differential

equations of the form $\dot{w}_i = f_i(w_1, w_2, w_3, w_4)$, for $i = 1, 2, 3, 4$, that could then be solved using conventional numerical methods [33], with initial conditions $w_i = 0$ at $t = 0$ for $i = 1, 2, 3, 4$. Nearly identical results to the full numerical solutions of Eqs. (4) and (5) were obtained (see, for example, Fig. 5), where comparisons were made by examining the connection due to Eqs. (7), (8), and $\theta = \omega t + \phi$.

However, for most of the conditions of Ref. [1], which examined A ranging up to about 1000 statvolt, and $a \approx 0.5\,\text{Å}$, we found that Eqs. (17) and (18) could be simplified yet further, allowing yet deeper analytical approximations. There are roughly three time scales involved in the above two equations, namely, $\tau = \frac{2e^2}{3mc^3} \approx 6.3 \times 10^{-24}$ sec (roughly the time for light to cross the distance of the classical electron radius of $r_e \equiv \frac{e^2}{mc^2}$, which is a key scaling quantity in the radiation reaction term), the period of the classical orbit, $T \equiv \frac{2\pi}{\omega} \approx 1.4 \times 10^{-16}$ sec for $a = 0.5\,\text{Å}$, and $T_s \equiv \frac{2\pi}{\omega_s}$, which we will call the period of the radial spiraling motion apparent in Fig. 1(a). From the numerical results in Ref. [1], Fig. 4, T_s became smaller as A became larger, with its value being about 1.4×10^{-14} sec when $A = 1000$ statvolt. Thus, $\omega_s \lesssim 7.4 \times 10^{13}$ sec^{-1}, while $\omega \approx 4.5 \times 10^{16}$ sec^{-1}, and $\frac{1}{\tau} \approx 1.6 \times 10^{23}$ sec^{-1}, so $\omega_s \ll \omega \ll \frac{1}{\tau}$ when $a \approx 0.5\,\text{Å}$ and $A < 1000$ statvolt. A simple check then of the terms in Eq. (18) reveals that according to these estimates, the $-2\omega\dot{\phi}$ and $-3\omega^2\frac{\delta}{a}$ terms should be the largest magnitude, with the $\frac{eA}{am}\sin(\phi - \alpha)$ term being the next most important, and followed last by the $\frac{\ddot{\delta}}{a}$ and $-2\omega^2\tau\frac{\dot{\delta}}{a}$ terms. Indeed, $\frac{\delta}{a} \approx -\frac{2}{3\omega}\dot{\phi}$ turns out to be a fairly good approximation, with

$$\frac{\delta}{a} = -\frac{2}{3\omega}\dot{\phi} - \frac{eA}{3am\omega^2}\sin(\phi - \alpha) \quad , \tag{19}$$

being a somewhat better approximation.

Substituting Eq. (19) into Eq. (17) then yields the following differential equation, all in terms of ϕ:

$$\ddot{\phi} + \frac{3eA}{am}\left(1 + \frac{2\dot{\phi}}{3\omega}\right)\cos(\phi - \alpha) - 3(\omega\tau)\omega^2 - 7(\omega\tau)\omega\dot{\phi} = 0 \quad . \tag{20}$$

Indeed, it turns out that Eq. (20), plus $\frac{\delta}{a} \approx -\frac{2}{3\omega}\dot{\phi}$, reproduces the results of Ref. [1] very nicely.

However, Eq. (20) is still fairly complicated; a further reduction can still be made that reveals a fair amount of insight. If we treat the terms of $\frac{2eA\dot{\phi}}{am\omega}\cos(\phi - \alpha)$ and $-7(\omega\tau)\omega\dot{\phi}$ as perturbation terms, then we should be able to obtain a reasonably close approximation

solution to Eq. (20) by the following version of the method of successive approximation, namely, where

$$\ddot{\phi}_0 + \frac{3eA}{am}\cos\left(\phi_0 - \alpha\right) - 3\left(\omega\tau\right)\omega^2 = 0 \tag{21}$$

yields the lowest order approximate solution, $\phi_0\left(t\right)$, with $\phi_0\left(t=0\right)=0$ and $\dot{\phi}_0\left(t=0\right)=0$, and then successive improvements to this solution are obtained by solving, for $n = 1, 2, ...,$

$$\begin{aligned}&\ddot{\phi}_n + \frac{3eA}{am}\cos\left(\phi_n - \alpha\right) - 3\left(\omega\tau\right)\omega^2 \\ &= -\frac{3eA}{am}\left(1 + \frac{2\dot{\phi}_{n-1}}{3\omega}\right)\cos\left(\phi_{n-1} - \alpha\right) + 7\left(\omega\tau\right)\omega\dot{\phi}_{n-1} \quad ,\end{aligned} \tag{22}$$

to enable one to deduce ϕ_1, ϕ_2, etc., with ϕ_n and $\dot{\phi}_n$ always set equal to zero at $t = 0$.

We will now make a few comparisons between the results of (i) Eqs. (21) combined with $\frac{\delta}{a} \approx -\frac{2}{3\omega}\dot{\phi}$, which we will call "case 0", to (ii) Eq. (20) combined also with $\frac{\delta}{a} \approx -\frac{2}{3\omega}\dot{\phi}$, which we will call "case P2" ("P" for perturbation), to "case E" ("E" for exact), meaning numerically solving Eqs. (4) and (5). Case P2 and case E are extremely close for most of the conditions of Ref. [1], with typical results looking almost identical to Fig. 5. [Cases P1 and P2 are essentially indistinguishable in Figs. 5 and 6(a), so we did not include their comparison in these figures. However, there are cases we will discuss shortly, where P2 is not fully adequate, and P1 is clearly the better approximation.] Hence, we can treat case P2 as yielding excellent agreement for times past the decay point, for most situations at least up to about $A \approx 1000$ statvolt, and for $a \approx 0.5\,\text{Å}$. In contrast, case 0 generally agrees with the other two cases only at the beginning (see Fig. 6), at which point it agrees very nicely [Fig. 6(b)]. Near the decay point [Fig. 6(c)], cases E and P2 are virtually still on top of each other, while case 0 remains of the same shape, unable to predict any tendency for decay.

Thus, case 0 provides a simplified basis for estimating the initial period and amplitude of the radial oscillations, while case P2 provides a basis for closely estimating the rate of increase in radial oscillation, and the time of decay, t_d. The difference between the two cases arises from the additional terms in Eq. (20) (case P2) which do not occur in Eq. (21) (case 0), namely,

$$\dot{\phi}\left[\frac{2}{3\omega}\cos\left(\phi - \alpha\right) - 7\omega^2\tau\right] \quad .$$

These terms make the amplitude in both the r vs. t curves, and in the ϕ vs. t curves, increase with time, and eventually give rise to the rapid change in orbital decay. These

terms also give rise to the slowly changing period of the radial oscillations.

What is interesting about the solution of Eq. (21), for case 0, is that it can be expressed in terms of the Legendre elliptic integral of the first kind. Indeed, if we drop the last term (the constant one) in Eq. (21), let $\alpha = \pi/2$, then the equation can be put in the same form as

$$\ddot{\Theta} + \left(\frac{g}{l}\right) \sin \Theta = 0 \quad , \tag{23}$$

which is the equation sometimes analyzed in mechanics textbooks as the full, nonlinear equation of motion for an idealized pendulum of length l, swinging with angular displacement Θ from the vertical, with a constant gravitational acceleration g acting. A nice discussion is provided in Ref. [34], Sec. 8.2, which shows the result as being an elliptic integral of the first kind.

Retaining the constant term in Eq. (21), however, provides a much closer match with cases P2 and E in the early time domain. The larger the amplitude A, then the less important this constant term. Multiplying Eq. (21) by $\dot{\phi}_0$, then integrating over t, enables one to show that

$$\frac{1}{2}\left(\dot{\phi}_0\right)^2 + \frac{3eA}{am} \sin\left(\phi_0 - \alpha\right) - 3\tau\omega^3\phi_0 = C \quad , \tag{24}$$

where C is a constant. (Again, ϕ_0 represents our "zero-order approximation" from Eq. (21), as opposed to the phase at $t = 0$.) In all our present examples, at $t = 0$, then $\phi_0 = \dot{\phi}_0 = 0$, so,

$$C = -\frac{3eA}{am} \sin\left(\alpha\right) \quad . \tag{25}$$

Solving for $\dot{\phi}_0$ and integrating once more, yields:

$$\frac{1}{2} \frac{1}{\left(\frac{3eA}{am}\right)^{1/2}} \int_{\phi_0(t_1)}^{\phi_0(t_2)} \frac{d\phi_0}{\left\{\frac{\tau\omega^3 am}{eA}\phi_0 - \left[\sin\left(\phi_0 - \alpha\right) + \sin\left(\alpha\right)\right]\right\}^{1/2}} = (t_2 - t_1) \quad . \tag{26}$$

This can be integrated numerically; in general, though, we are not aware of a closed form solution, unless one treats the $\frac{\tau\omega^3 am}{eA}\phi_0$ as sufficiently small that it can be ignored. Again, for large A, this is a good approximation. In that case, one then has available the elliptic integral solutions [35]. A better approximation, is to treat the term $\frac{\tau\omega^3 am}{eA}\phi_0$ as a small term and to expand the integrand, thereby obtaining a power series in the dimensionless

parameter $\frac{\tau\omega^3 am}{eA}$. We obtain:

$$(t_2 - t_1) = \frac{1}{2\left(\frac{3eA}{am}\right)^{1/2}} \left\{ \begin{array}{c} \int\limits_{\phi_0(t_1)}^{\phi_0(t_2)} \frac{d\phi_0}{\{-\sin(\phi_0-\alpha)-\sin(\alpha)\}^{1/2}} \\ -\frac{1}{2}\frac{\tau\omega^3 am}{eA} \int\limits_{\phi_0(t_1)}^{\phi_0(t_2)} \frac{\phi_0 d\phi_0}{\{-\sin(\phi_0-\alpha)-\sin(\alpha)\}^{3/2}} + O\left[\left(\frac{\tau\omega^3 am}{eA}\right)^2\right] \end{array} \right\} \quad . \tag{27}$$

The first integral can be evaluated using integral # 2.5711 in Ref. [35], which gives the result as a Legendre elliptic integral of the first kind; the second integral appears to be not readily expressible in terms of standard integrals, and must be numerically evaluated.

Still, if one only wants to estimate and extract some information quickly, such as the initial amplitude and the initial period, then Eqs. (21), (24), and (25) provides sufficient information. If we evaluate Eq. (24) at the first minimum (ϕ_0 starts at 0, falling first, then continuing in a periodic motion up and down), we obtain

$$\sin\left(\alpha - \phi_0\left(T_s/2\right)\right) + \frac{am\tau\omega^3}{eA}\phi_0\left(T_s/2\right) = \sin\left(\alpha\right) \quad , \tag{28}$$

where T_s represents the period. This is a nonlinear relationship for $\phi_0\left(T_s/2\right)$ that can be readily solved. Treating $\left(\frac{am\tau\omega^3}{eA}\right)$ as a small parameter, for large A, then an iterative method suggests itself where

$$\left(\phi_0\right)_{n+1} = \alpha - \sin^{-1}\left[\sin\left(\alpha\right) - \frac{am\tau\omega^3}{eA}\left(\phi_0\right)_n\right] \quad . \tag{29}$$

At the first minimum, with $\left[\phi_0\left(T_s/2\right)\right]_1 = -2\pi$, then

$$\left[\phi_0\left(T_s/2\right)\right]_2 = \alpha - \sin^{-1}\left[\sin\left(\alpha\right) + \frac{2\pi am\tau\omega^3}{eA}\right] \quad , \tag{30}$$

yields fairly good results for the first minima of ϕ_0, with rapid improvement coming by increasing iterations of Eq. (29). Since $\phi_0\left(t=0\right) = 0$, then $\left|\left[\phi_0\left(T_s/2\right)\right]_2\right|$ is the approximate amplitude of the oscillations of ϕ_0. As can be seen from Eq. (30), or more generally from Eq. (28), this amplitude is a highly nonlinear function of A, as first illustrated in Fig. 4 in Ref. [1].

The approximate period can then be extracted either from a numerical integration of Eq. (26), letting $t_1 = 0$, $t_2 = T_s/2$, $\phi_0\left(t_1\right) = 0$, $\phi_0\left(t_2\right) = \phi_0\left(T_s/2\right)$ as obtained above; alternatively, one could obtain a more approximate, but analytic and closed form result, using the first integral in Eq. (27). We have found that numerical results for T_s from

this approximate method, yield good agreement with the full solution of Eqs. (4) and (5), particularly for smaller values of $\left(\frac{am\tau\omega^3}{eA}\right)$, although, our testing only examined the situation where eA is still small compared to the magnitude of the Coulombic binding force.

Figures 7(a) and (b) shows some of the subtle, but significant differences in the ϕ_0 behavior due to changes in A and α. Again, ϕ_0 largely dictates the initial behavior of the full particle behavior, meaning, that by writing $x(t) = [a + \delta(t)]\cos(\theta)$, $y(t) = [a + \delta(t)]\sin(\theta)$, and by approximating $\theta \approx \omega t + \phi_0(t)$, with $\delta(t) \approx -\frac{2a}{3\omega}\dot{\phi}_0 - \frac{eA}{3m\omega^2}\sin(\phi_0 - \alpha)$, then one "usually" (we will qualify this shortly) obtains a fairly good approximation to the initial behavior, including amplitude and period of the full r versus t curves as calculated from Eqs. (4) and (5) [see Fig. 6(b)]. As seen in Fig. 7, simply changing α has a very significant effect on the amplitude of ϕ_0, as well as a less significant, but still important, effect on the period.

To put some of this in perspective, Fig. 8 shows, for initial radius 0.5 Å, $A = 1000$ statvolt, the variety of solutions one obtains by simply changing the initial phase α between the orbiting electron and the electric field direction. Figure 8(a) shows a sketch indicating the meaning of α, namely, that at $t = 0$, if $\alpha = 0$, then the force $(-e)\,\mathbf{E}_{\text{plane}}$ of the plane wave in the $x - y$ plane is parallel to the initial velocity of the particle. Even though initially the frequency of the plane wave and the orbital frequency of the particle are chosen to be the same, this changes immediately for $\alpha = 0$, since the plane wave acts to accelerate the electron, making it spiral outward, increasing its radius, and changing its orbital frequency. Figure 8(b) shows the behavior as α ranges between $-\pi/2$ to 0, and 0 to $\pi/2$, while Fig. 8(c) shows the complementary region as α ranges between $-\pi/2$ to $-\pi$, and π (physically equivalent to $-\pi$) to $+\pi/2$. As noted in Ref. [2], increasing A can significantly increase the length of time of stability; here we also see that for a fixed value of A, with $A > \frac{2e^3\omega}{3mc^3a^2}$, the initial phase α has a very similar and significant effect.

What is rather surprising is that when $\alpha = -\pi$ (or π), so that the initial force $(-e)\,\mathbf{E}_{\text{plane}}$ is exactly *opposite* to the initial velocity $\mathbf{v}$ of the particle, decay does *not* automatically occur; instead, near-immediate decay begins when $\alpha \approx -\pi/2$, as can be seen in Figs. 8(b) and 8(c) [as is also predicted by the corresponding $\phi_0(t)$ vs. t curve in Fig. 7(b)]. Moreover, when $\alpha = -\pi$, the time to decay is nearly identical, although not exactly [see Fig. 8(d)], to the situation of $\alpha = 0$, when $(-e)\,\mathbf{E}_{\text{plane}}$ and $\mathbf{v}$ are initially parallel, at least for $A = 1000$ statvolt. Indeed, each of the curves in Fig. 8(b) have a very similar nature (*i.e.*, shape and time to decay) to the curves in Fig. 8(c), with $\frac{5}{8}\pi$ similar to $\frac{3}{8}\pi$, $\frac{3}{4}\pi$ to $\frac{1}{4}\pi$, $\frac{7}{8}\pi$ to $\frac{1}{8}\pi$, etc., as

indicated in Fig. 8(a). More specifically, for $A = 1000$ statvolt, any initial angle in the top half of the dotted circle in Fig. 8(a) that produces one of the curves in Fig. 8(b), will result in a value of t_d very similar to the corresponding initial angle that is its mirror reflection about the horizontal line in Fig. 8(a) [Fig. 8(c)].

The following discussion attempts to shed some physical insight into the reasons for these nonintuitive effects. As can be seen in Fig. 8(e), immediately after $t = 0$, the radius increases for the $\alpha = 0$ case and decreases for the $\alpha = -\pi$ case. The same is true for each pair of angles discussed above; *i.e.*, each of the trajectories with an angle α from the top half of the dotted circle in Fig. 8(a) has the radius initially increasing, while the mirror image about the horizontal [*e.g.*, the "mirror" of $(1/8)\,\pi$ is $(7/8)\,\pi$] has the radius initially decreasing. In the first case $(-e)\,\mathbf{E}_{\rm plane}$ acts to accelerate the particle, while in the latter, $(-e)\,\mathbf{E}_{\rm plane}$ deaccelerates it, thereby explaining why r tends to increase (decrease) for the initial angles in the top (bottom) half of the dotted circle in Fig. 8(a).

However, the reason why decay does not immediately set in for the $\alpha = -\pi$ case, is that when the particle deaccelerates, this allows the $(-e)\,\mathbf{E}_{\rm plane}$ force, which is rotating at a fixed angular frequency rate of ω, to catch up to the orbiting particle, which then starts to aid the particle's orbit to increase. The amplitudes of oscillation of the r versus t curves in Fig. 8(e) are nearly identical. Again, this property holds fairly closely for every pair of mirror image angles mentioned above. However, these two physically different situations do not have exactly the same amplitude for $A = 1000$ statvolt; numerical calculations reveals that the $\alpha = \pi$ amplitude in Fig. 8(e) is about 0.01% *larger* than the corresponding initial $\alpha = 0$ amplitude [see Fig. 8(f)]. This difference in initial amplitude is what helps to explain the difference in time for orbital decay [Fig. 8(d)] to set in for these two curves. After all, as noted in both Refs. [1] and [2], the common phenomena observed when quasi-stability is established by a plane wave (or set of plane waves in the elliptical case) acting to oppose the radiation reaction effect, is that the amplitude of oscillation of the spiralling in and out orbits, steadily increases until orbital decay finally occurs.

Figure 8(g) zooms in on Fig. 8(c) to reveal this pattern of increasing amplitude, leading to orbital decay. Not all of the different curves of α are shown here, in order to make sure the general pattern is evident. What is interesting, is that each of the curves are very similar in character (*i.e.*, shape and size). Indeed, by translating them, and superimposing them at the transition point, one can obtain a fairly close match - not exact, as there are

differences, but, the similarity is quite apparent, as seen in Fig. 8(h).

Finally, it seems natural to ask why the $\alpha = \pi/2$ curve does not decay immediately, and in fact lasts the longest of all curves (for $A \gg A_c$), while the $\alpha = -\pi/2$ curve results in nearly immediate decay. However, we will save fully addressing this point for a subsequent article, as it seems that the easiest way to discuss it is to go through an analysis that reveals that for each value of $A > A_c$, there are two values of α that result in t_d actually being infinite. One of those values of α turns out to be "stable" and the other "unstable"; by this we mean that in the "stable" case, a small deviation in α still results in t_d being very large, while in the "unstable" case, a small deviation in α results in $t_d \to 0$. For $A \gg A_c$, the stable and unstable values of α can be shown to be $\alpha \approx +\pi/2$ and $\alpha \approx -\pi/2$, respectively. Our future article will help explain these points.

However, here we can show how subtle the analysis can be for some of these points by clarifying a statement made earlier, that "usually" case 0 produces the initial behavior quite well. For smaller values of A, case 0 does work well, even at $\alpha = +\pi/2$; however, by $A = 1000$ statvolt, then near the critical junction of $\alpha \approx +\pi/2$, the initial prediction for case 0 does not match case E, nor does case P2 match case E very well. The terms dropped between cases P1 and P2, namely, the second, third, and fourth terms in Eq. (17), become no longer negligible for this situation. Near $t = 0$ in this situation, the first and last terms in Eq. (17) are very comparable in magnitude, as are the second and third, while the fourth term involving the $\dot{\delta}$ term is very small. The end result, for this large a value of A is that, as shown in Fig. 9, the radius actually increases once, before falling into an oscillatory deceasing pattern.

Thus, there can be a subtle interplay between the interaction between δ and $\dot{\phi}$. As seen in Fig. 9, decay does not immediately begin for the $A = 1000$ statvolt, $\alpha = +\pi/2$ case, as r first undergoes a small increase, then decay begins. However, for $A = 100$ statvolt, decay begins immediately, as seen in Fig. 9(b) in Ref. [1]. This transitory behavior for the $\alpha = \pi/2$, $A = 1000$ statvolt case is not predicted by the case P2 case, but is well predicted by case P1. For most other situations, for $\alpha \neq \pi/2$, and for A up to at least 1000 statvolt ($a \approx 0.5\,\text{Å}$), case P2 provides a sufficiently accurate and simple explanation of the orbiting particle motion.

IV. CONCLUDING REMARKS

The key point made in Ref. [1] was that the stability of circular orbital motion for a classical electron about a classical nucleus can be maintained for extended lengths of time, not just by one carefully selected circularly polarized plane wave, but by a large range of amplitudes of plane waves, provided that the amplitude satisfies $A \geq \frac{2e^3\omega_c}{3mc^3a^2} = A_c$. We are not aware of this fact being noted before. Reference [2] then extended this observation to the more general case of elliptical motion. A very similar condition was shown to occur in the elliptical case as in the circular one, although now a family of plane waves was required, with frequencies consisting of harmonics of the orbital motion. However, once their amplitudes had been selected, then scaling all the amplitudes by a constant factor would again allow a long stability condition to be achieved.

The present article turned to a different point, namely, that not only the amplitude of the incident waves, but also their phase with respect to the orbital motion of the classical electron, is quite important. The phase of a circularly polarized electromagnetic plane wave can have subtle and profound effects on the stability of the orbit of the classical charged particle. What is most surprising is that the phase can vary enormously and one can still obtain quasistability; the issue is not so much that quasistability will be obtained, but rather, how long it can be achieved. Indeed, as will be shown in future work, for any value of the electric field amplitude of the incident plane wave, provided that $A \geq A_c$, one can always find a value of α, the angle between the velocity vector and $(-e)\,\mathbf{E}$, such that the orbit *never* decays (for the NR equations of motion addressed here for circular motion). Also, as will be shown in this future work, a deeper physical understanding can be obtained for the wide range of decay time as the initial phase is varied, and why this range depends so significantly on the ratio A/A_c.

The aim of the perturbation work investigated here was to shed deeper insight into some of the key trends that have been observed in our studies on the classical hydrogen atom interacting with simple states of classical electromagnetic radiation. In particular, here we analyzed the steady increase in amplitude of the oscillating radius versus time curves and the rapid change of character of this oscillating behavior to one of orbital decay. By expanding the radius and frequency into their small variational components, simpler nonlinear differential equations were obtained that gave rise to these key features. Moreover,

as shown in Sec. II, these characteristics for r vs. t carry over in many ways to other traditional variables of interest, such as the energy and angular momentum of the classical hydrogen atom.

Our belief is that the detailed study of such effects, in combination with other work in progress on multi-plane wave effects, will provide much greater insight regarding the dynamical and statistical possibilities of the classical hydrogen atom being in thermodynamic equilibrium with electromagnetic radiation. Moreover, this research should aid in understanding the interaction of the classical hydrogen atom with applied radiation that makes deviations to that equilibrium, as done in spectroscopy situations. Indeed, work of ours [30], [29] reveal that a probability density distribution of the electron's position, obtained by classical simulations like those reported here, but with approximations made to the classical electromagnetic zero-point spectrum, result in a strikingly close approximation to the prediction of Schrödinger's equation for hydrogen in its ground state. We expect to be able to report and provide yet deeper analysis on these results in the near future.

ACKNOWLEDGEMENTS

We thank Prof. Timothy Boyer for reading the first draft of this article and for his encouragement and helpful suggestions.

---

[1] D. C. Cole and Y. Zou. Simulation study of aspects of the classical hydrogen atom interacting with electromagnetic radiation: Circular orbits. *Journal of Scientific Computing*, 2004. , Accepted for publication (expected publication date is Feb. 2004). Preprint available at http://www.bu.edu/simulation/publications/dcole/publications.html.

[2] D. C. Cole and Y. Zou. Simulation study of aspects of the classical hydrogen atom interacting with electromagnetic radiation: Elliptical orbits. *Journal of Scientific Computing*, 2004. , Accepted for publication (expected publication date is mid-2004). Preprint available at http://www.bu.edu/simulation/publications/dcole/publications.html.

[3] J. Grochmalicki, M. Lewenstein, and K. Rzazewski. Stabilization of atoms in superintense laser fields: Is it real? *Phys. Rev. Lett.*, 66(8):1038–1041, 1991.

[4] J. A. Griffiths and D. Farrelly. Ionization of rydberg atoms by circularly and elliptically polarized microwave fields. *Phys. Rev. A*, 45(5):R2678–R2681, 1992.

[5] P. A. Braun. Discrete semiclassical methods in the theory of rydberg atoms in external fields. *Rev. Mod. Phys.*, 65(1):115–161, 1993.

[6] W. Clark and C. H. Greene. Adventures of a rydberg electron in an anisotropic world. *Rev. Mod. Physics*, 71(3):821–833, 1999.

[7] S. Yoshida, C. O. Reinhold, P. Kristofel, and J. Burgdorfer. Exponential and nonexponential localization of the one-dimensional periodically kicked rydberg atom. *Phys. Rev. A*, 62:023408, 2000.

[8] C. Wesdorp, F. Robicheaux, and L. D. Noordam. Displacing rydberg electrons: The monocycle nature of half-cycle pulses. *Phys. Rev. Lett.*, 87(8):083001, 2001.

[9] A. Muthukrishnan and Jr. Stroud, C.R. Entanglement of internal and external angular momenta of a single atom. *Journal of Optics B: Quantum and Semiclassical Optics*, 4:S73, 2002.

[10] D.J. Tannor and S.A. Rice. Control of selectivity of chemical reaction via control of wave packet evolution. *Journal of Chemical Physics*, 83:5013, 1985.

[11] P. Brumer and M. Shapiro. Control of unimolecular reactions using coherent light. *Chemical Physics Letters*, 126:541, 1986.

[12] T. H. Boyer. Scaling symmetry and thermodynamic equilibrium for classical electromagnetic radiation. *Found. Phys.*, 19:1371–1383, 1989.

[13] D. C. Cole. Classical electrodynamic systems interacting with classical electromagnetic random radiation. *Found. Phys.*, 20:225–240, 1990.

[14] T. H. Boyer. Conformal symmetry of classical electromagnetic zero-point radiation. *Found. Physics*, 19(4):349–365, 1989.

[15] T. W. Marshall. Random electrodynamics. *Proc. R. Soc. London, Ser. A*, 276:475–491, 1963.

[16] T. W. Marshall. Statistical electrodynamics. *Proc. Camb. Phil. Soc.*, 61:537–546, 1965.

[17] T. H. Boyer. Derivation of the blackbody radiation spectrum without quantum assumptions. *Phys. Rev.*, 182:1374–1383, 1969.

[18] T. H. Boyer. Classical statistical thermodynamics and electromagnetic zero-point radiation. *Phys. Rev.*, 186:1304–1318, 1969.

[19] T. H. Boyer. Random electrodynamics: The theory of classical electrodynamics with classical electromagnetic zero–point radiation. *Phys. Rev. D*, 11(4):790–808, 1975.

[20] H. E. Puthoff. Ground state of hydrogen as a zero-point-fluctuation-determined state. *Phys. Rev. D*, 35(10):3266–3269, 15 May 1987.

[21] H. M. Franca, H. Franco, and C. P. Malta. A stochastic electrodynamics interpretation of spontaneous transitions in the hydrogen atom. *Eur. J. Phys.*, 18:343–349, 1997.

[22] D. C. Cole. Derivation of the classical electromagnetic zero–point radiation spectrum via a classical thermodynamic operation involving van der waals forces. *Phys. Rev. A*, 42:1847–1862, 1990.

[23] D. C. Cole. World Scientific, Singapore, 1993. pp. 501–532 in compendium book, "Essays on Formal Aspects of Electromagnetic Theory," edited by A. Lakhtakia.

[24] L. de la Peña and A. M. Cetto. *The Quantum Dice - An Introduction to Stochastic Electrodynamics*. Kluwer Acad. Publishers, Kluwer Dordrecht, 1996.

[25] T.W. Marshall and P. Claverie. Stochastic electrodynamics of nonlinear systems. i. particle in a central field of force. *Journal of Mathematical Physics*, 21(7):1819–25, July 1980.

[26] P. Claverie, L. Pesquera, and F. Soto. Existence of a constant stationary solution for the hydrogen atom problem in stochastic electrodynamics. *Physics Letters A*, 80A(2-3):113–16, 24 Nov. 1980.

[27] P. Claverie and F. Soto. Nonrecurrence of the stochastic process for the hydrogen atom problem in stochastic electrodynamics. *Journal of Mathematical Physics*, 23(5):753–9, May 1982.

[28] J. S. Rigden. *Hydrogen: The Essential Element*. Harvard University Press, Cambridge, Massachusetts, 2002.

[29] D. C. Cole and Y. Zou. Analysis of orbital decay time for the classical hydrogen atom interacting with circularly polarized electromagnetic radiation. 2004. Accepted for publication in Phys. Rev. E. Preprint available at http://www.bu.edu/simulation/publications/dcole/publications.html.

[30] D. C. Cole and Y. Zou. Quantum mechanical ground state of hydrogen obtained from classical electrodynamics. *Physics Letters A*, 317(1–2):14–20, Oct. 13, 2003. Preprint available at http://www.bu.edu/simulation/publications/dcole/publications.html.

[31] C. Teitelboim, D. Villarroel, and Ch. G. van Weert. Classical electrodynamics of retarded fields and point particles. *Riv. del Nuovo Cimento*, 3(9):1–64, 1980.

[32] D. C. Cole. Cross–term conservation relationships for electromagnetic energy, linear momentum, and angular momentum. *Found. Phys.*, 29(11):1673–1693, 1999.

[33] W. H. Press, S. A. Teukolsky, W. T. Vetterling, and B. P. Flannery. *Numerical Recipes in*

C: The Art of Scientific Computing. Cambridge University Press, New York, second edition, 1992.

[34] T. L. Chow. *Classical Mechanics*. John Wiley & Sons, Inc., New York, 1995.

[35] I. S. Gradshteyn and I. M. Ryzhik. *Tables of Integrals, Series, and Products,*. Academic, New York, 1980.

Figure Captions

Figure 1: r vs. t for the $A = 100$ statvolt CP plane wave case, but with the initial phase between $\mathbf{E}$ and $\dot{\mathbf{z}}$ being $-\pi/4$. Also shown is the $A = 0$ curve, which shows orbital decay right at the beginning. (a) the r vs. t simulations are carried out to $t = 5 \times 10^{-12}$ sec. (b) Zoomed-in view of (a), near the decay-transition point. The envelope continues to grow until decay sets in. (c) The region near the transition point is blown-up further to show the details of the behavior.

Figure 2: (a) $E = \frac{1}{2}m\mathbf{v}^2 - \frac{e^2}{r}$ vs. t over the same region as in Fig. 1(a), again with $A = 100$ statvolt; (b) E vs. t over the same region as in Fig. 1(c), near the transition point; (c) $L_z = m\left(\dot{x}y - \dot{y}x\right)$ vs. t over the same region as in Fig. 1(a); (d) L_z vs. t over the same region as in Fig. 1(c). Although a bit difficult to see, if 2(a) and 2(c) were blown up as in Fig. 1(b), the same increase in envelope curve would be seen. Note that in Figs. 2(c) and 2(d) the magnitude of $|L_z|$ decreases after the transition point occurs, since $L_z < 0$.

Figure 3: The same situation as in Fig. 1 with $A = 100$ statvolt, but now: (a) total Lorentz force due to the plane wave, plus the radiation reaction, along the tangential direction of the velocity of the particle, versus t. It's magnitude does not change radically at the transition point; rather, the pattern of the force curve undergoes a sharp transition; (b) the total force vs. t and E vs. t, superimposed. When the tangential force equals zero, so that no work per time is being done on the particle, then E hits either a minimum or maximum.

Figure 4: Same situation as in Fig. 1, with $A = 100$ statvolt, $\alpha = -\pi/4$, but now different regions blown up for plots of $(\theta - \omega t)$, where $x = r\cos\theta$, $y = r\sin\theta$, and ω is the angular frequency of the CP plane wave. (a) Here the dramatic change in $(\theta - \omega t)$ is revealed at the transition (orbital-decay) point. Prior to this point, $(\theta - \omega t)$ oscillates within a comparatively narrow band, as seen in 4(b). However, the envelope of this band steadily increases. In 4(c), the peaks of $(\theta - \omega t)$ widen as the transition point is approached.

Figure 5: Numerical solutions to Eqs. (4) and (5) for r vs. t is compared to the numerical solutions to the approximate equations of motion of Eqs. (17) and (18), where $r = a + \delta(t)$ and $\theta = \phi + \omega t$, and $A = 100$ statvolt and $\phi = -\pi/4$. If, for example, the same region as in Fig. 1(c) was blown up, the difference between the two numerical results would not be detectable by eye. Only near $t \gtrsim 4.5 \times 10^{-12}$ sec does the difference become discernible. If θ was plotted as in Fig. 4, for the two methods, again, only near $t \gtrsim 4.5 \times 10^{-12}$ sec would

the difference become evident.

Figure 6: r vs. t for Case 0 [Eq. (21) combined with $\frac{\delta}{a} = -\frac{2}{3\omega}\dot{\phi}$], Case P2 [Eq. (20) combined with $\frac{\delta}{a} = -\frac{2}{3\omega}\dot{\phi}$], and Case E [Eqs. (4) and (5)]. In Figs. 6(a), 6(b), and 6(c), Cases P2 and E are virtually on top of each other, except for $t \gtrsim 4.5 \times 10^{-12}$ in 6(a). In Fig. 6(b), at the beginning, Case 0 matches Cases P2 and E very well, although one can see the period and amplitude of P2 and E increasing as t becomes larger. In Fig. 6(c), Case 0 continues on with no change in shape.

Figure 7: ϕ_0 vs. t [Eq. (21)] when the initial radius is 0.5 Å, and for different conditions of the phase α. (a) $A = 100$ statvolt. (b) $A = 1000$ statvolt. Note that the time scale on the $A = 1000$ statvolt plot only goes up to 2.6×10^{-14} sec, as the period of the $A = 1000$ curves is much shorter than the $A = 100$ statvolt case. With this scaling, (a) and (b) look similar, but, there are differences. As can be seen, both the amplitude and period of ϕ_0 change with α, with the amplitude being more strongly effected than the period; the amplitude is nearly zero at $\alpha = +\pi/2$, but increases in magnitude as α changes from $+\pi/2$, to $+3\pi/8$, to $\pi/4$, to 0, to $-\pi/4$, to $-3\pi/8$. [See Figs. 8(a) and 11(a) for greater clarification of these trends.] However, by the point that $\alpha = -\pi/2$, then ϕ_0 no longer undergoes an oscillatory behavior in time, as orbital decay sets in almost immediately, as seen in Fig. 8.

Figure 8: (a) A diagram showing the meaning of the values of α in the other plots here, namely, α is the angle between the velocity $\mathbf{v}$ and the force $(-e)\,\mathbf{E}_{\rm plane}$ of the plane wave acting on the electron at time $t = 0$. When $\alpha = 0$, $\mathbf{v}$ and $(-e)\,\mathbf{E}$ are initially parallel. For $A \gg A_c$, the initial phase $\alpha \approx -\pi/2$ has the smallest value of t_d and $\alpha \approx +\pi/2$ has the largest t_d. Pairs of angles like $-\pi/4$, $-3\pi/4$, or $+\pi/4$, $+3\pi/4$, or 0, π, have values of t_d very similar, when $A = 1000$ statvolt. For smaller values of A, these "mirror angles" no longer behave similarly, as will be analyzed more deeply in later work. Figs. 8(b) through 8(g) show various plots of r vs. t for $A = 1000$ statvolt, all with initial radius 0.5 Å. (b) r vs. t for different values of α ranging from $-\pi/2$ to 0, and 0 to $+\pi/2$ [top part of (a)]; (c) r vs. t for α ranging from $-\pi/2$ to $-\pi$ and π to $\pi/2$ [bottom part of (a)]; (d) r vs. t, comparing the difference in the $\alpha = 0$ and $\alpha = \pi$ curves at the point of decay; (e) r vs. t, comparing the difference in the $\alpha = 0$ and $\alpha = \pi$ curves initially; (f) initial behavior, as in (e), but now over a longer time period; (g) a blown up view of (c), right near $r = 0.5$ Å. Here, the increase in amplitude of each of the curves can readily be seen. (h) The r vs. t curves for $\alpha = \frac{3}{8}\pi$, $\frac{1}{4}\pi$, 0, $-\frac{1}{4}\pi$, $-\frac{3}{8}\pi$, $-\frac{1}{2}\pi$, each translated in time and superimposed on each other to

show the similarity in shape at the point of transition.

Figure 9: The initial transitory behavior of r vs. t for the $\alpha = -\pi/2$ case with $A = 1000$ statvolt is shown here. Case P1 still accurately represents the exact case, E, but the approximations of cases P2 and 0 are quite different initially from E. It should be noted that for $A = 100$ statvolt, these curves would again all lie on top of each other. Thus, an initial transitory behavior is revealed here as A becomes sufficiently large for the $\alpha = -\pi/2$ case, before the spiraling decay sets in.

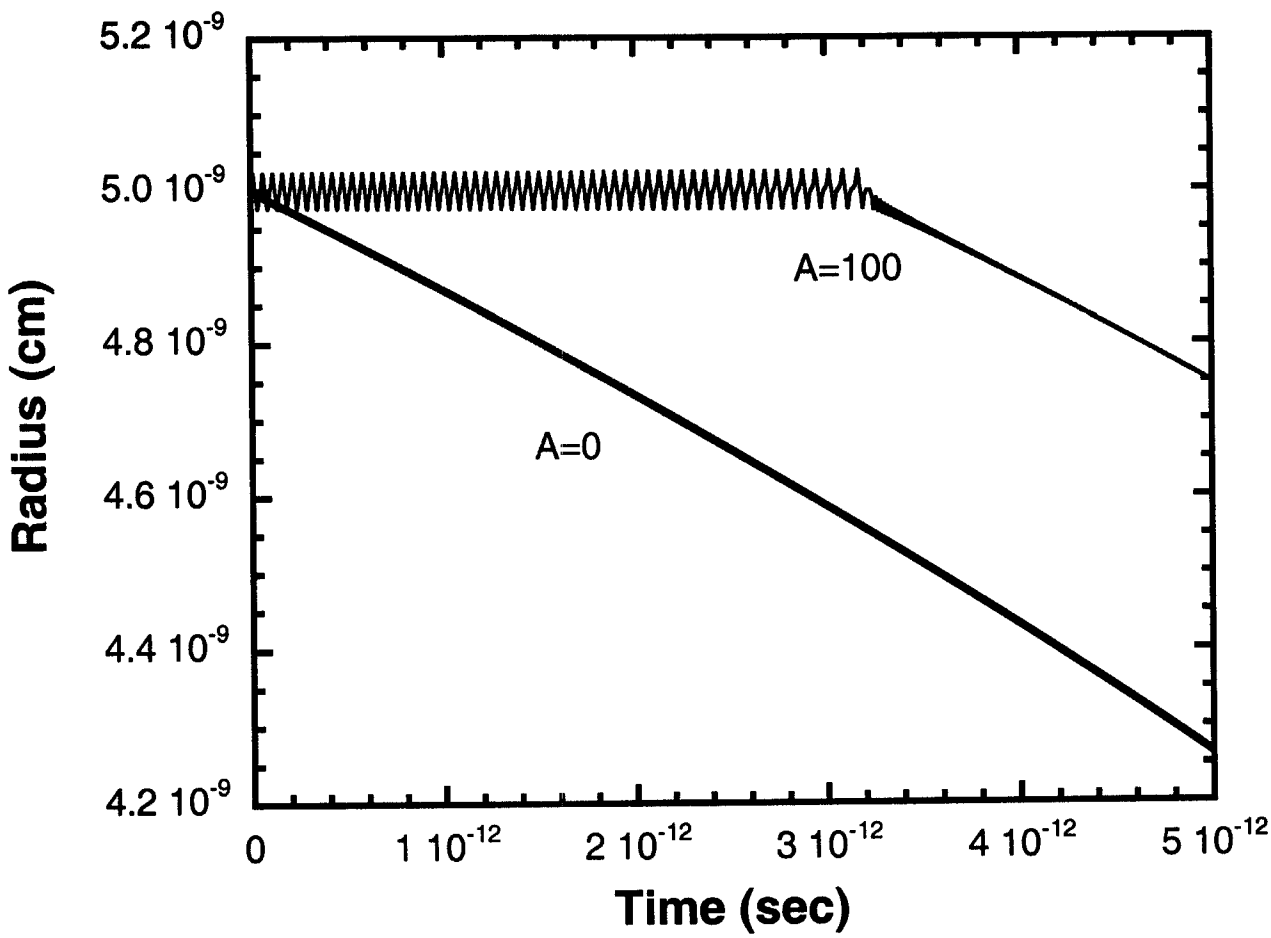
5.2 10-9
5.0 10-9
4.8 10-9
4.6 10-9
4.4 10-9
4.2 10-9
Radius (cm)
A=100
A=0
0
1 10-12
2 10-12
3 10-12
4 10-12
5 10-12
Time (sec)

Fig. 1(a)

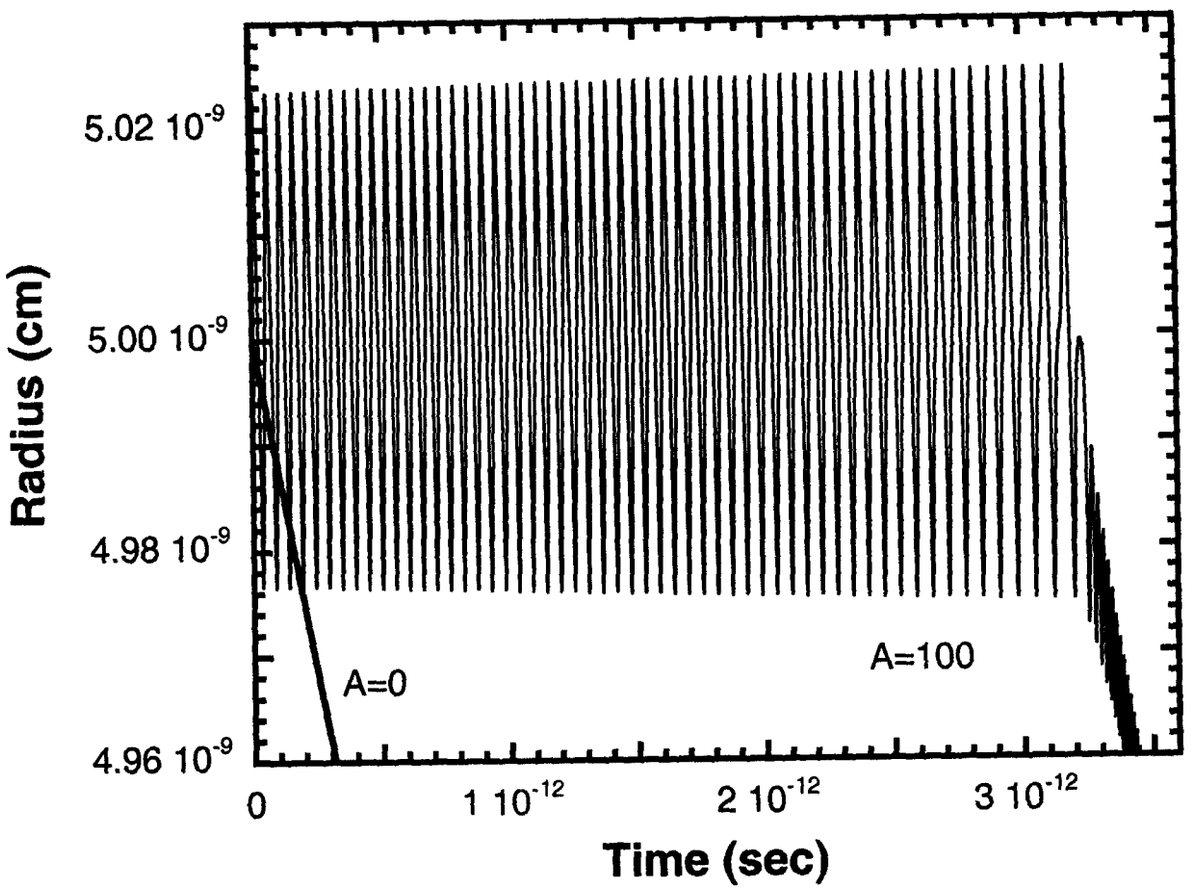
Radius (cm)
5.02 10-9
5.00 10-9
4.98 10-9
4.96 10-9
A=0
A=100
0
1 10-12
2 10-12
3 10-12
Time (sec)

Fig. 1(b)

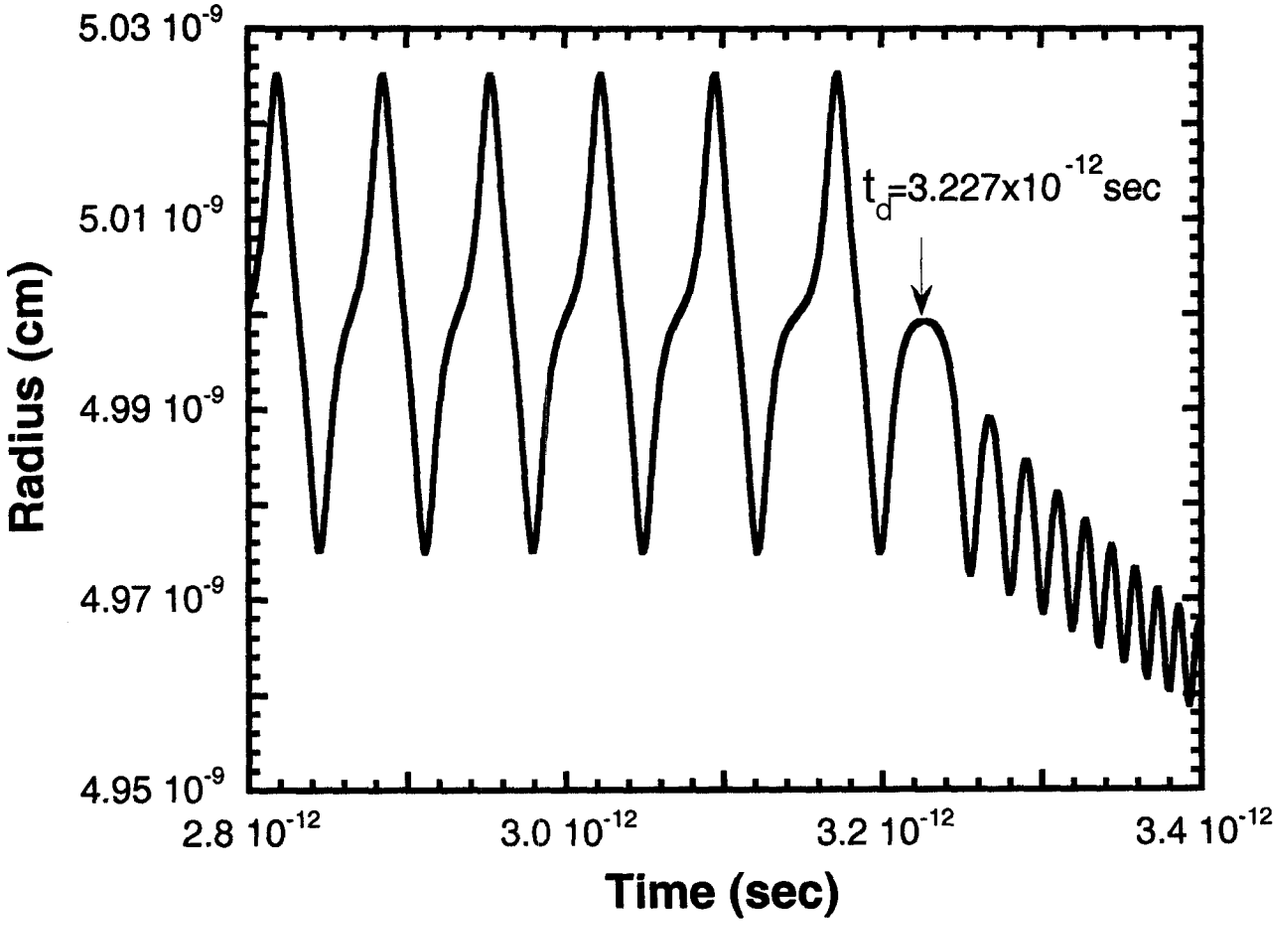
5.03 10-9
5.01 10-9
4.99 10-9
4.97 10-9
4.95 10-9
Radius (cm)
td=3.227x10-12sec
2.8 10-12
3.0 10-12
3.2 10-12
3.4 10-12
Time (sec)

Fig. 1(c)

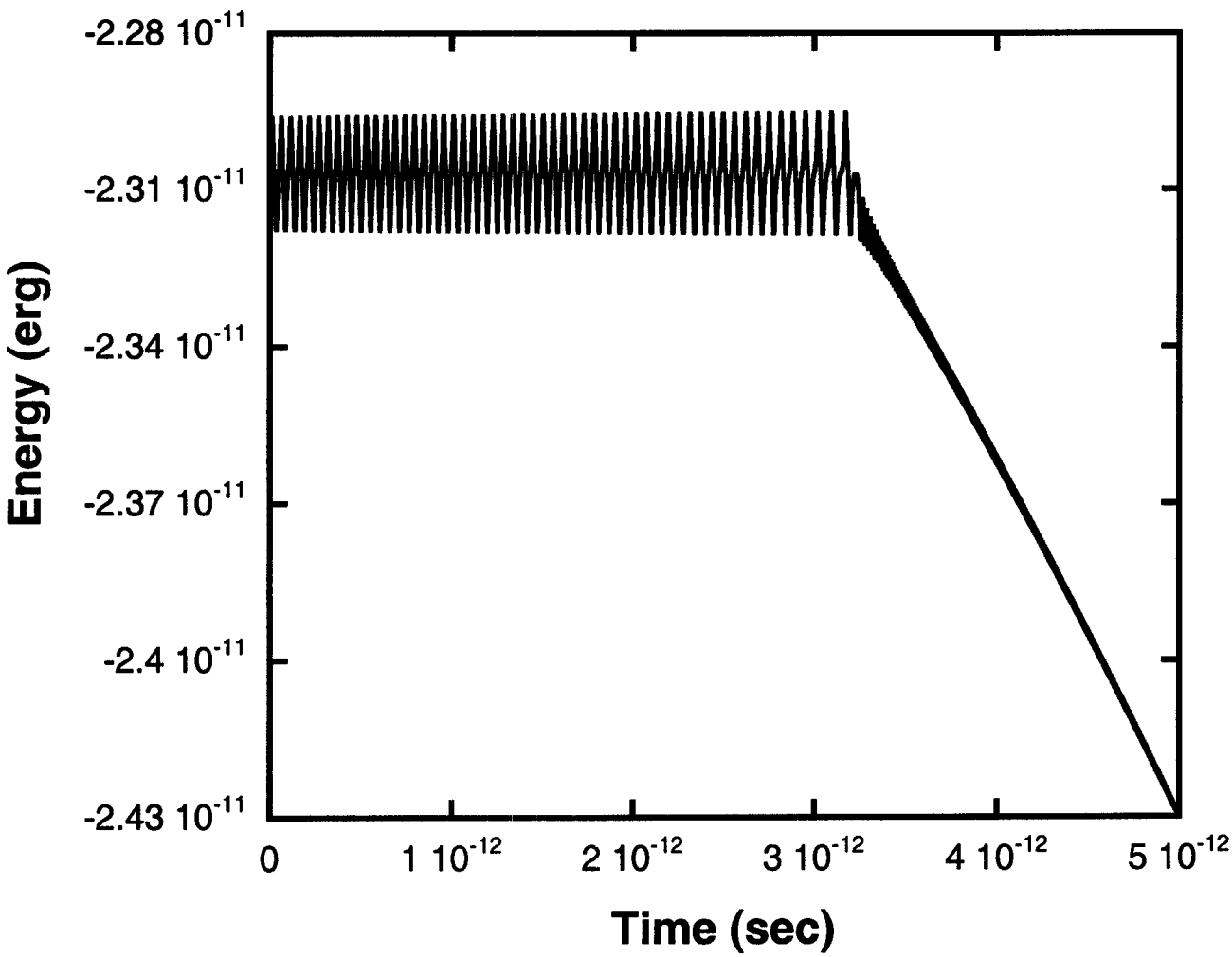
-2.28 10^-11
-2.31 10^-11
-2.34 10^-11
-2.37 10^-11
-2.4 10^-11
-2.43 10^-11
Energy (erg)
0
1 10^-12
2 10^-12
3 10^-12
4 10^-12
5 10^-12
Time (sec)

Fig. 2(a)

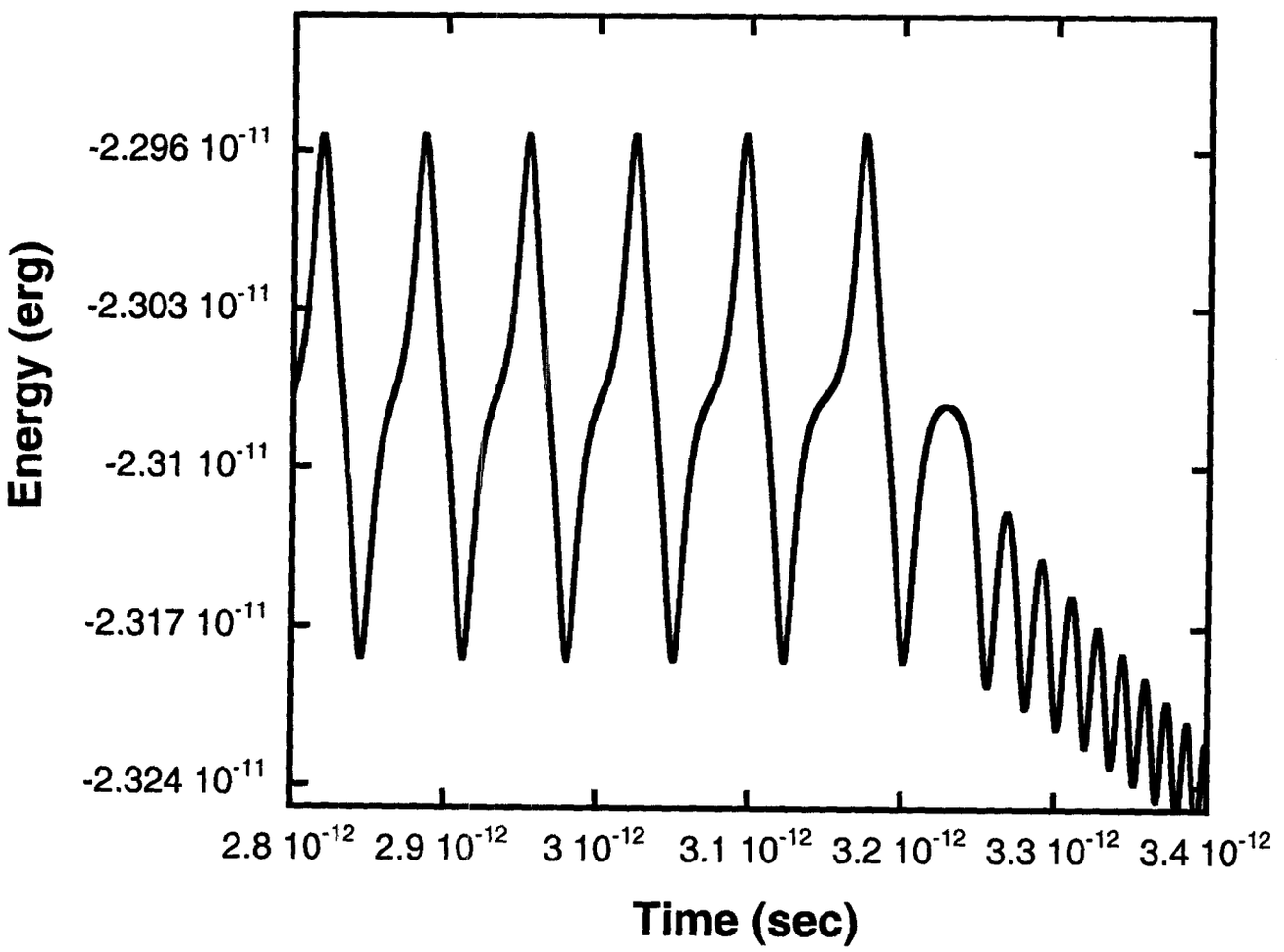
Energy (erg)
-2.296 10^-11
-2.303 10^-11
-2.31 10^-11
-2.317 10^-11
-2.324 10^-11
2.8 10^-12
2.9 10^-12
3 10^-12
3.1 10^-12
3.2 10^-12
3.3 10^-12
3.4 10^-12
Time (sec)

Fig. 2(b)

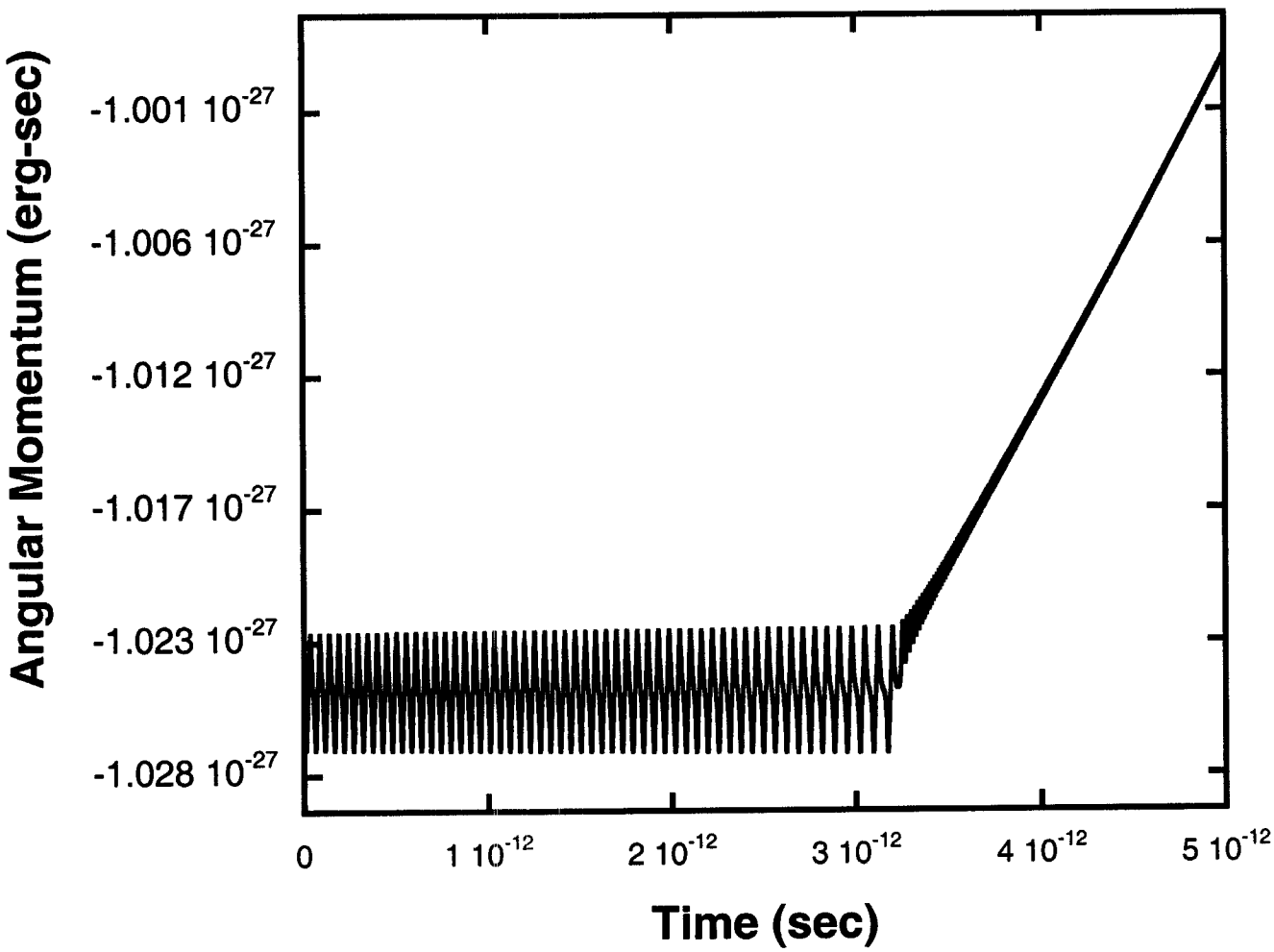
Angular Momentum (erg-sec)
-1.001 10-27
-1.006 10-27
-1.012 10-27
-1.017 10-27
-1.023 10-27
-1.028 10-27
0
1 10-12
2 10-12
3 10-12
4 10-12
5 10-12
Time (sec)

Fig. 2(c)

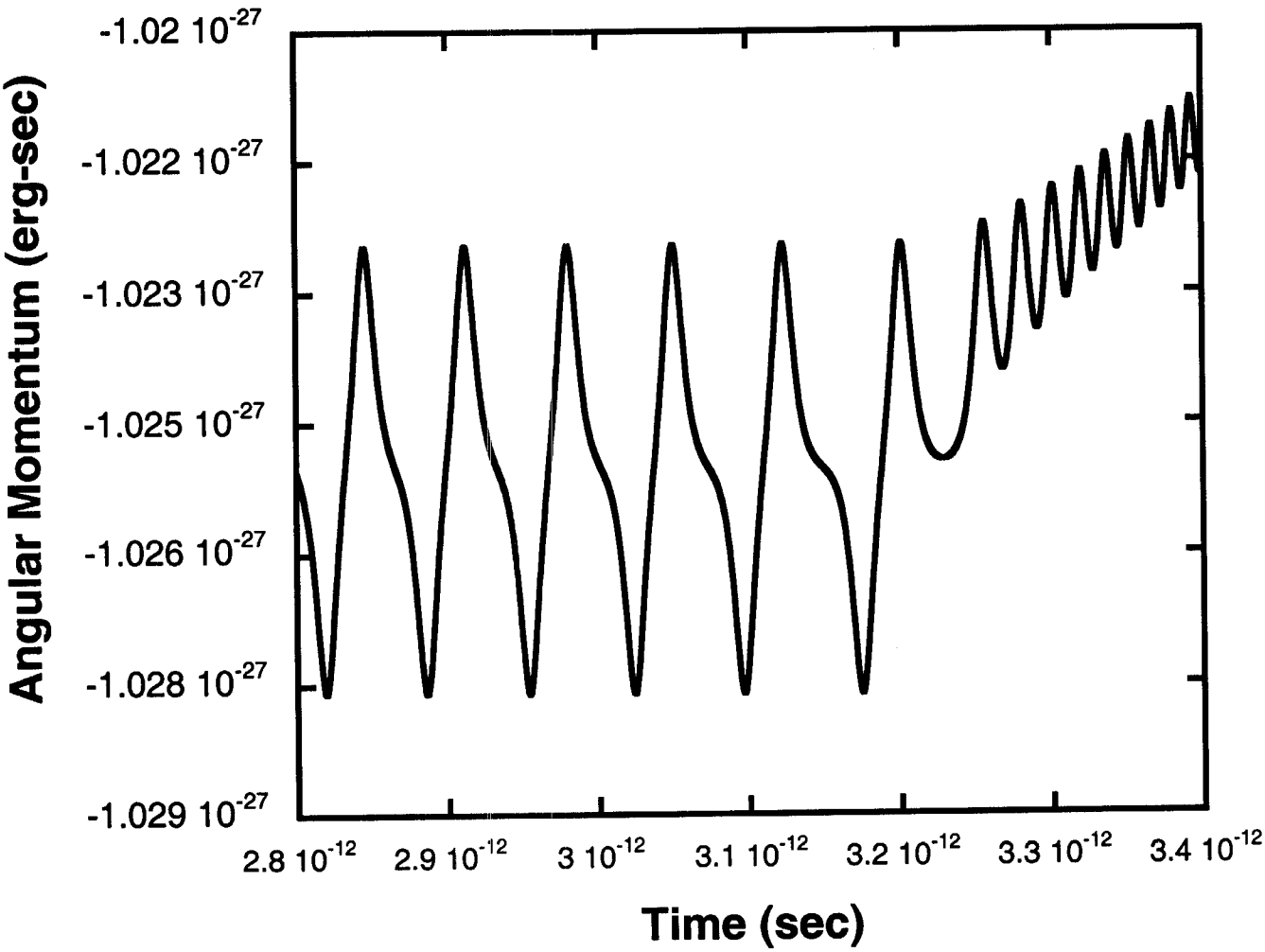
-1.02 10^-27
-1.022 10^-27
-1.023 10^-27
-1.025 10^-27
-1.026 10^-27
-1.028 10^-27
-1.029 10^-27
Angular Momentum (erg-sec)
2.8 10^-12
2.9 10^-12
3 10^-12
3.1 10^-12
3.2 10^-12
3.3 10^-12
3.4 10^-12
Time (sec)

Fig. 2(d)

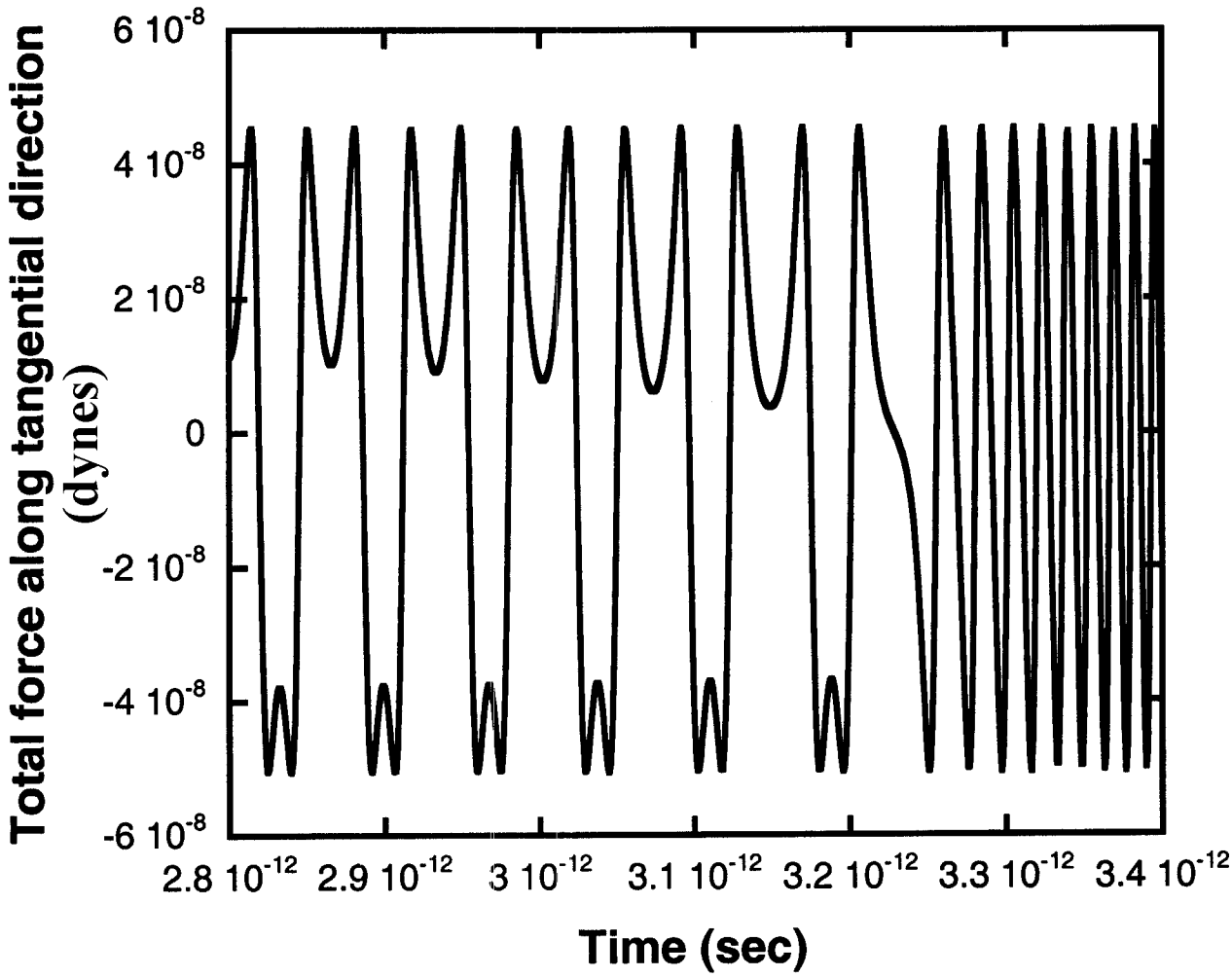
Total force along tangential direction (dynes)
6 10-8
4 10-8
2 10-8
0
-2 10-8
-4 10-8
-6 10-8
2.8 10-12
2.9 10-12
3 10-12
3.1 10-12
3.2 10-12
3.3 10-12
3.4 10-12
Time (sec)

Fig. 3(a)

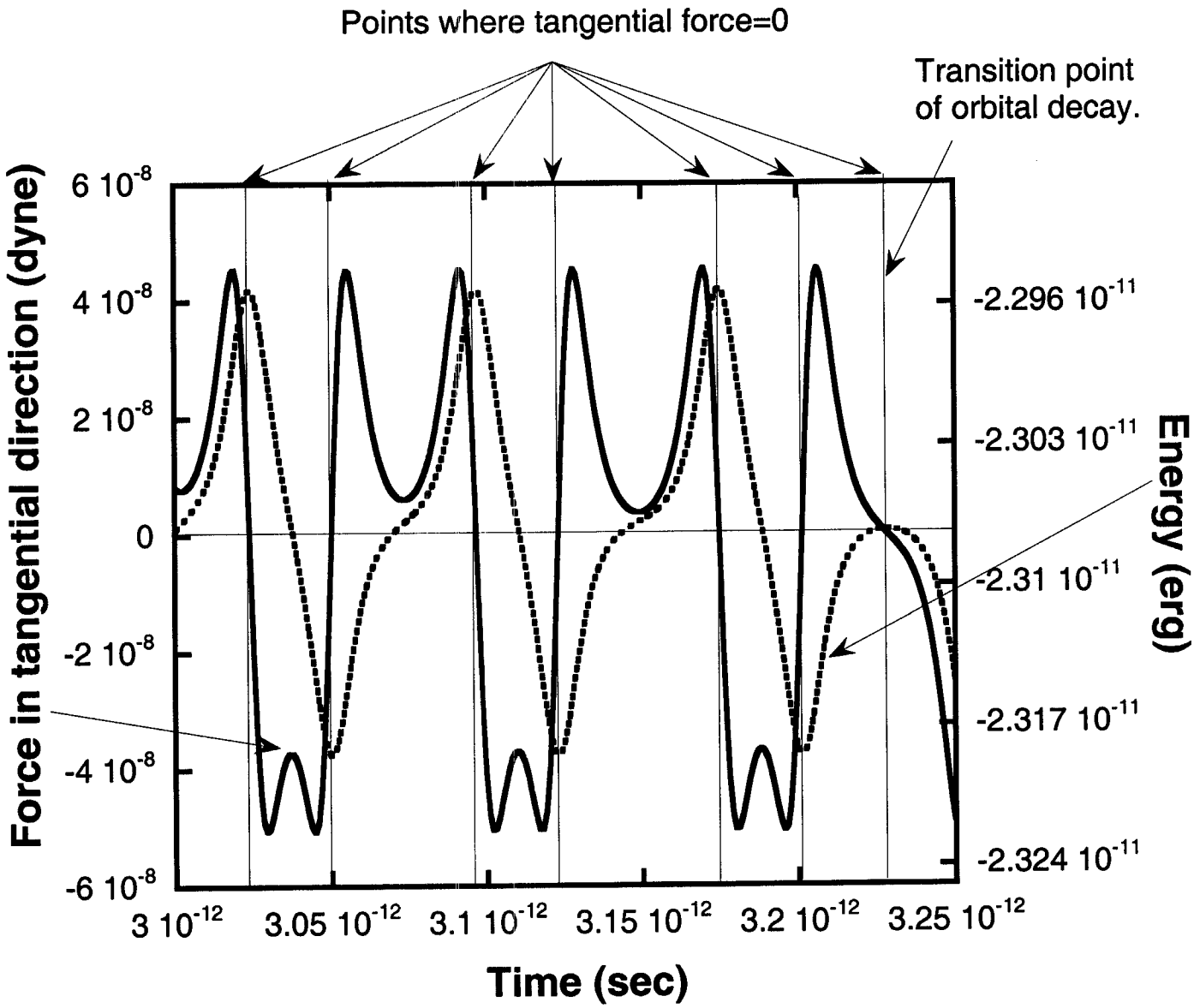
Points where tangential force=0
Transition point
of orbital decay.
Force in tangential direction (dyne)
6 10-8
4 10-8
2 10-8
0
-2 10-8
-4 10-8
-6 10-8
-2.296 10-11
-2.303 10-11
-2.31 10-11
-2.317 10-11
-2.324 10-11
Energy (erg)
3 10-12
3.05 10-12
3.1 10-12
3.15 10-12
3.2 10-12
3.25 10-12
Time (sec)

Fig. 3(b)

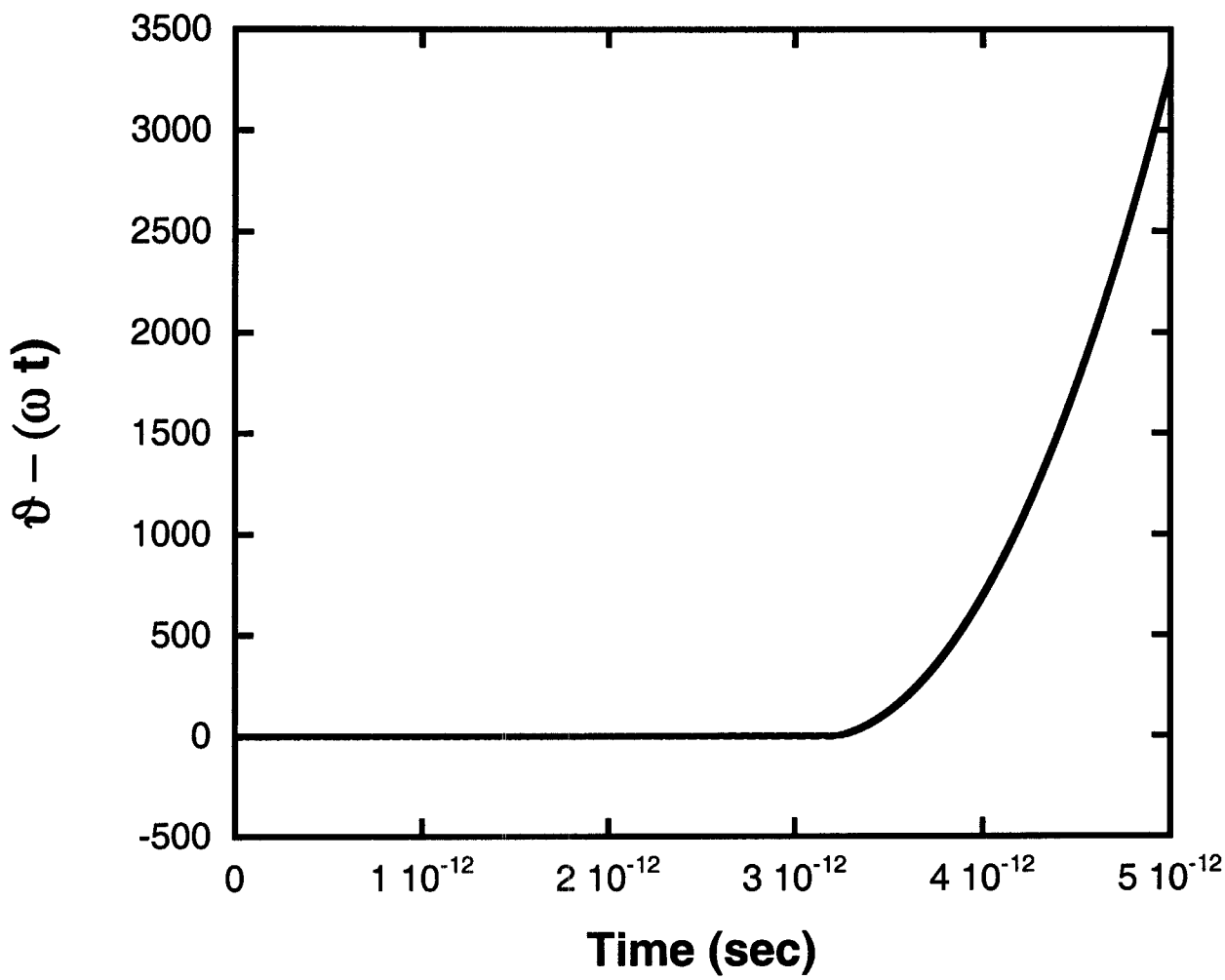
3500
3000
2500
2000
1500
1000
500
0
-500
$\vartheta - (\omega t)$
0
$1\ 10^{-12}$
$2\ 10^{-12}$
$3\ 10^{-12}$
$4\ 10^{-12}$
$5\ 10^{-12}$
Time (sec)

Fig. 4(a)

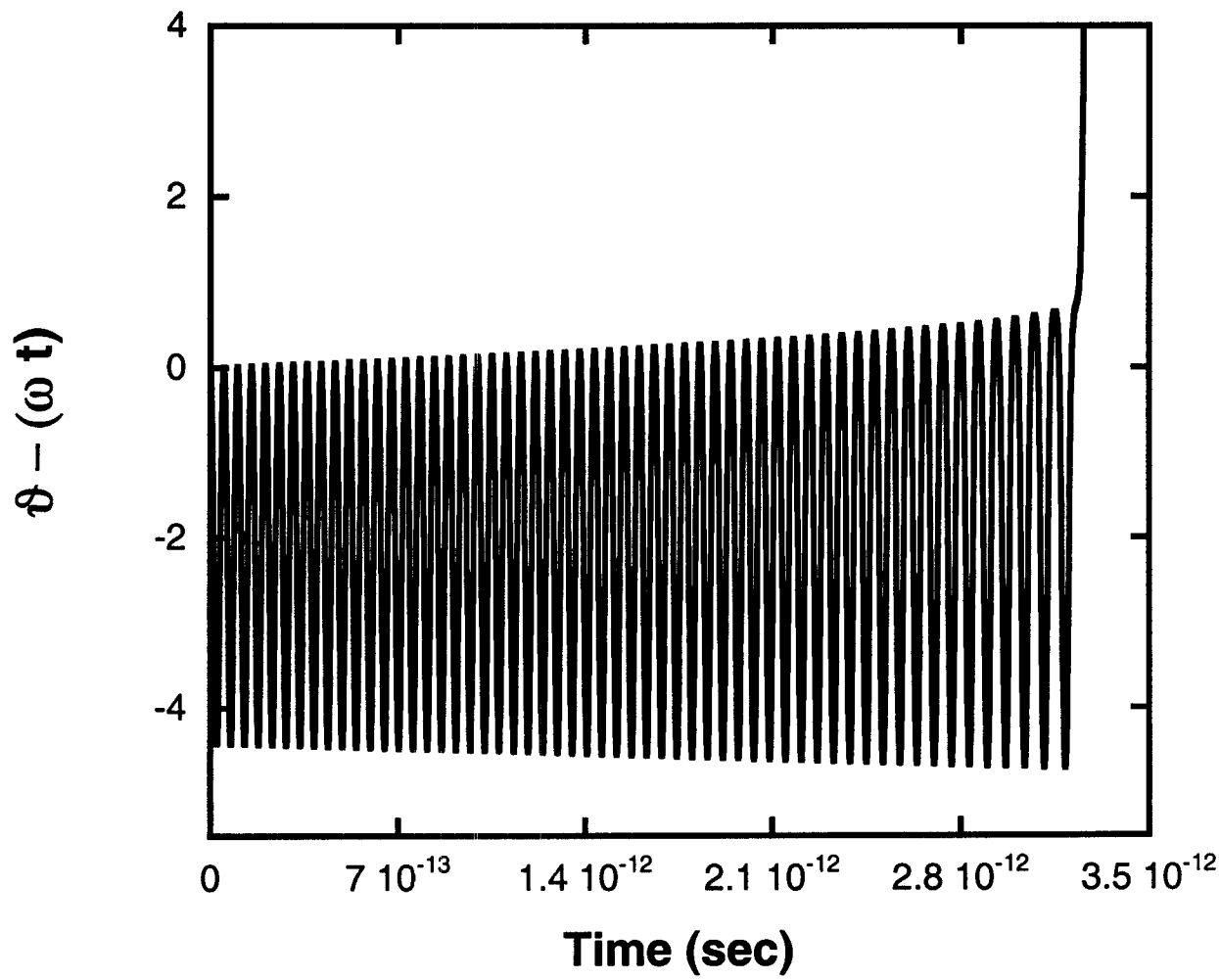

Fig. 4(b)

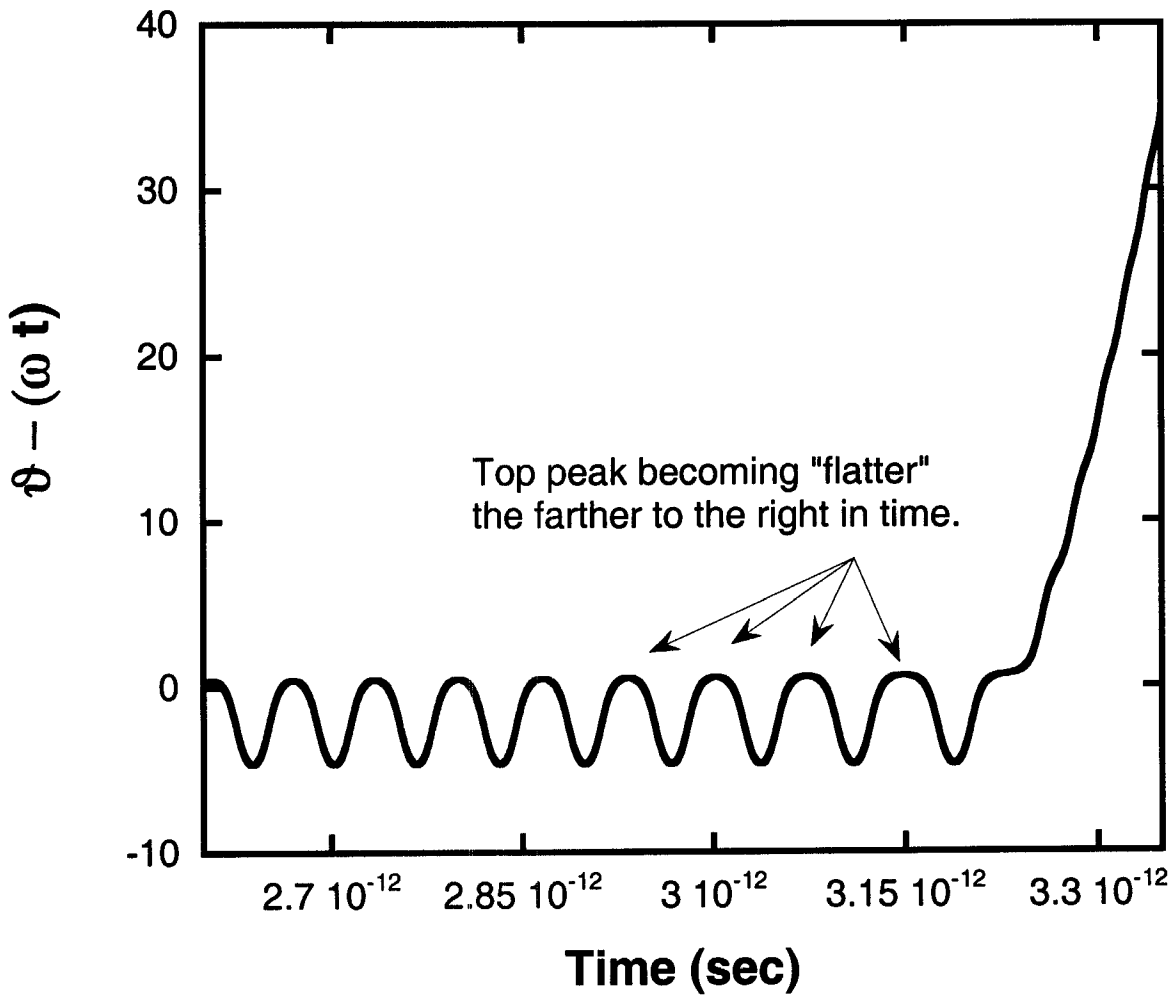
40
30
20
10
0
-10
ϑ – (ω t)
Top peak becoming "flatter"
the farther to the right in time.
2.7 10-12
2.85 10-12
3 10-12
3.15 10-12
3.3 10-12
Time (sec)

Fig. 4(c)

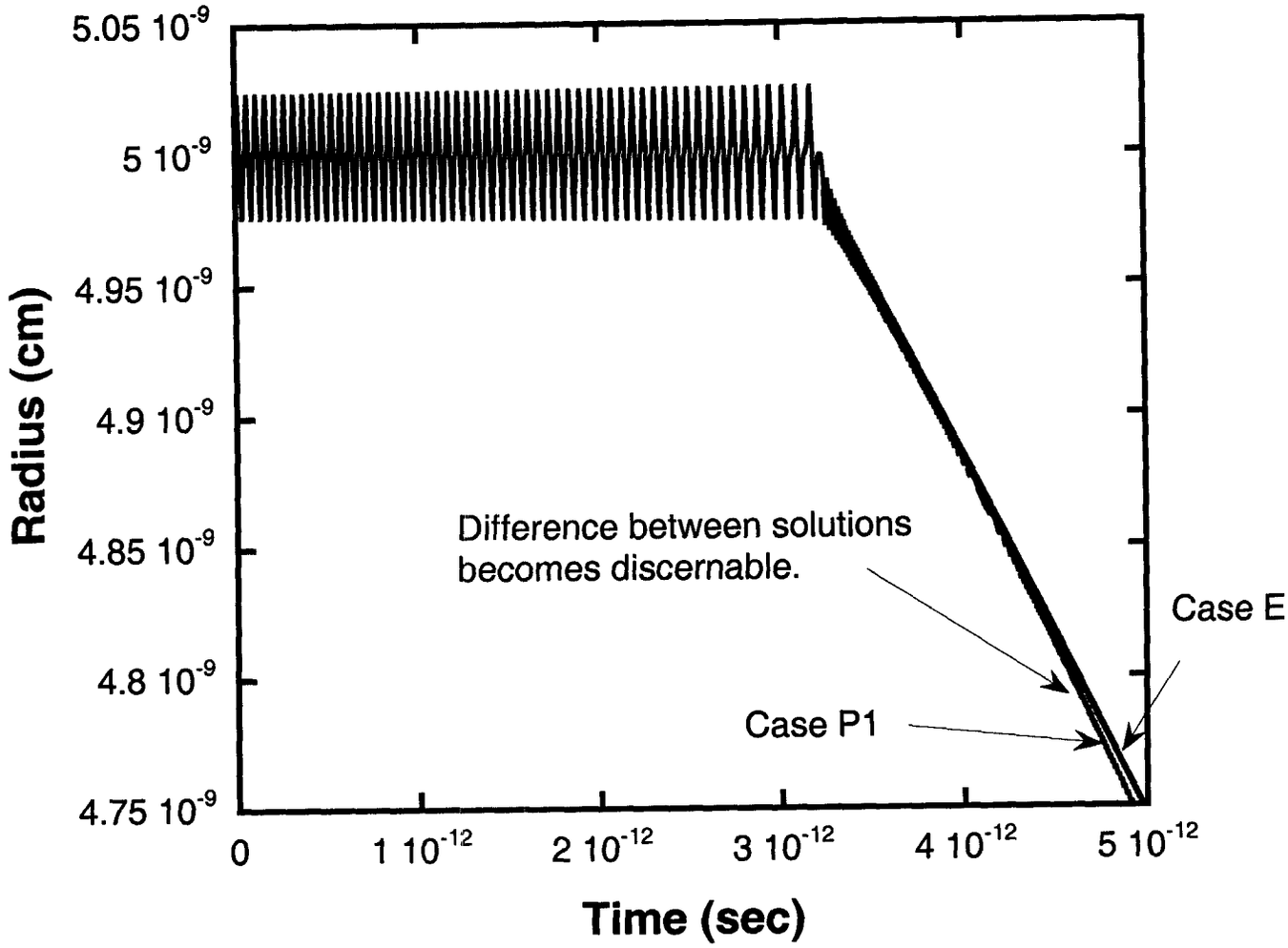
5.05 10-9
5 10-9
4.95 10-9
4.9 10-9
4.85 10-9
4.8 10-9
4.75 10-9
Radius (cm)
0
1 10-12
2 10-12
3 10-12
4 10-12
5 10-12
Time (sec)
Difference between solutions becomes discernable.
Case E
Case P1

Fig. 5

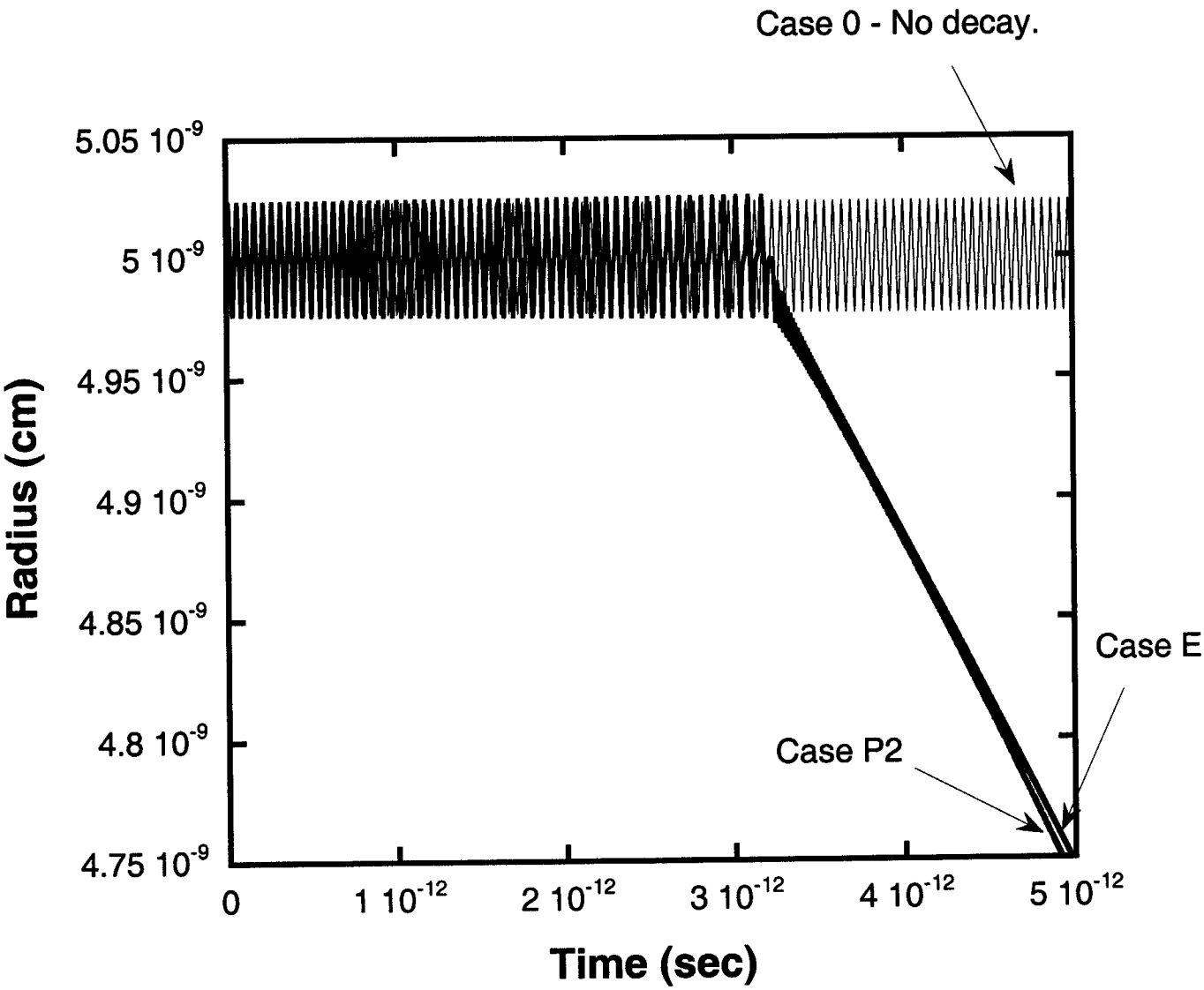
Case 0 - No decay.
5.05 10-9
5 10-9
4.95 10-9
4.9 10-9
4.85 10-9
4.8 10-9
4.75 10-9
Radius (cm)
0
1 10-12
2 10-12
3 10-12
4 10-12
5 10-12
Time (sec)
Case E
Case P2

Fig. 6(a)

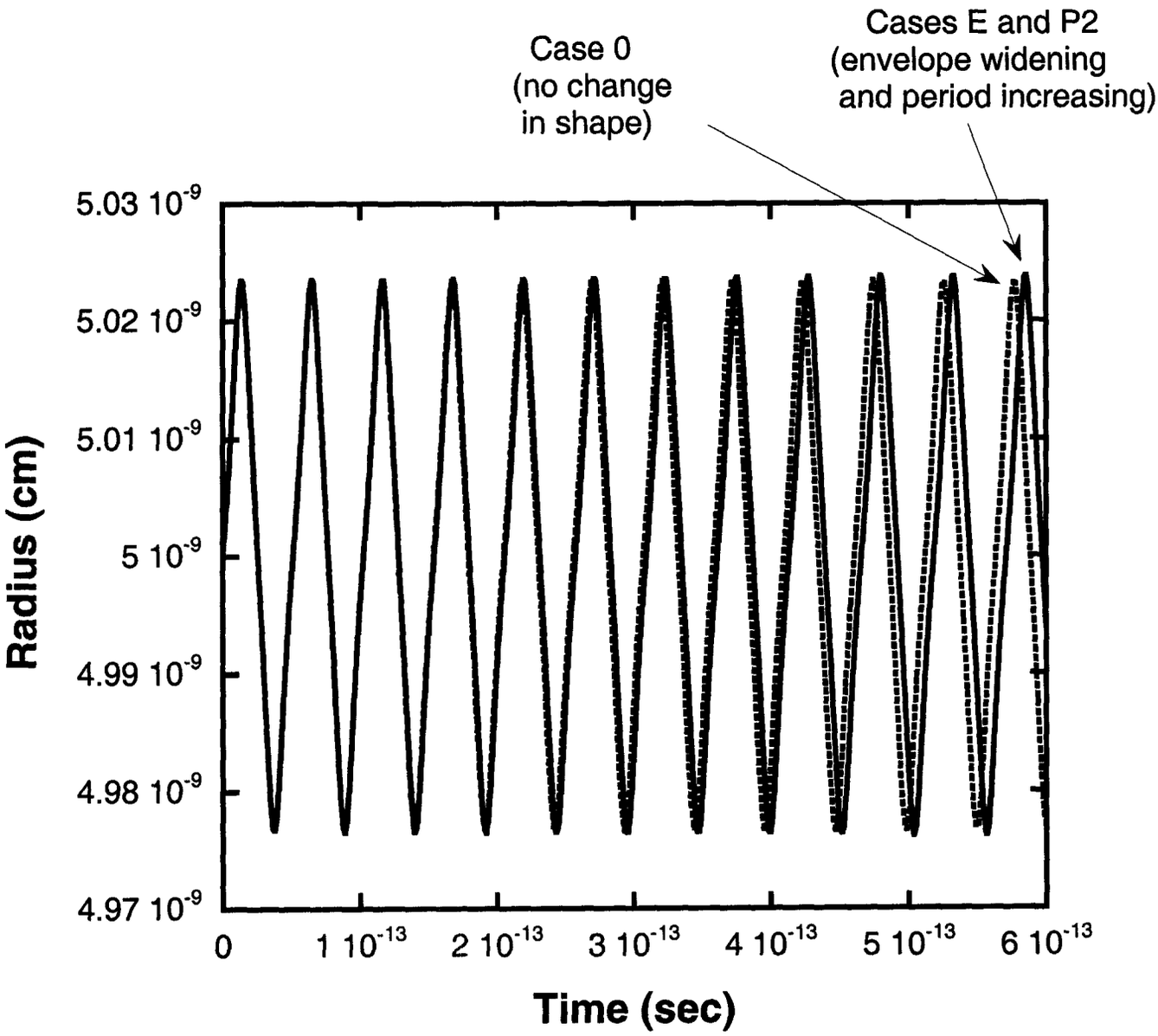
Case 0
(no change
in shape)
Cases E and P2
(envelope widening
and period increasing)
5.03 10-9
5.02 10-9
5.01 10-9
5 10-9
4.99 10-9
4.98 10-9
4.97 10-9
Radius (cm)
0
1 10-13
2 10-13
3 10-13
4 10-13
5 10-13
6 10-13
Time (sec)

Fig. 6(b)

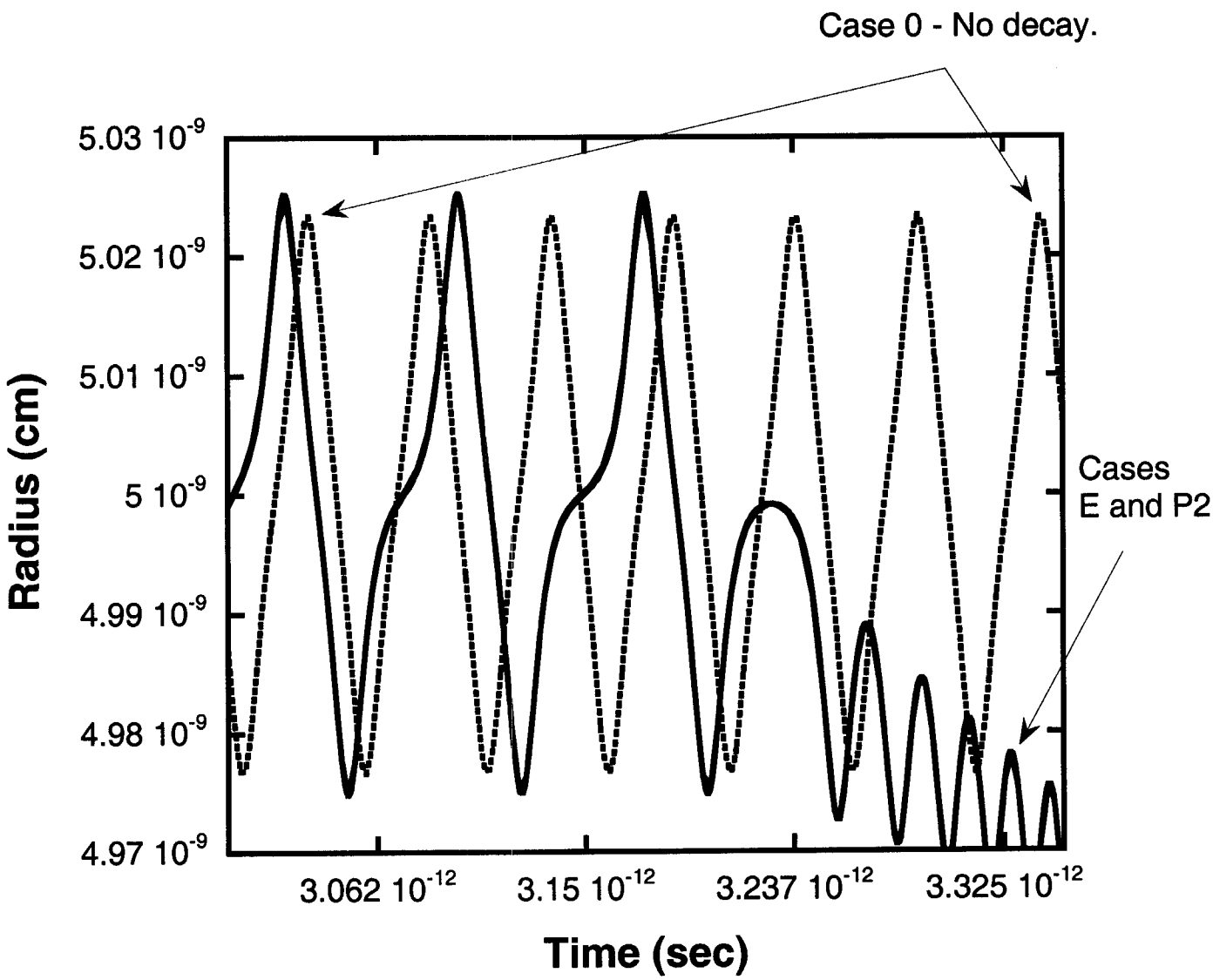
Case 0 - No decay.
Cases
E and P2
Radius (cm)
5.03 10-9
5.02 10-9
5.01 10-9
5 10-9
4.99 10-9
4.98 10-9
4.97 10-9
3.062 10-12
3.15 10-12
3.237 10-12
3.325 10-12
Time (sec)

Fig. 6(c)

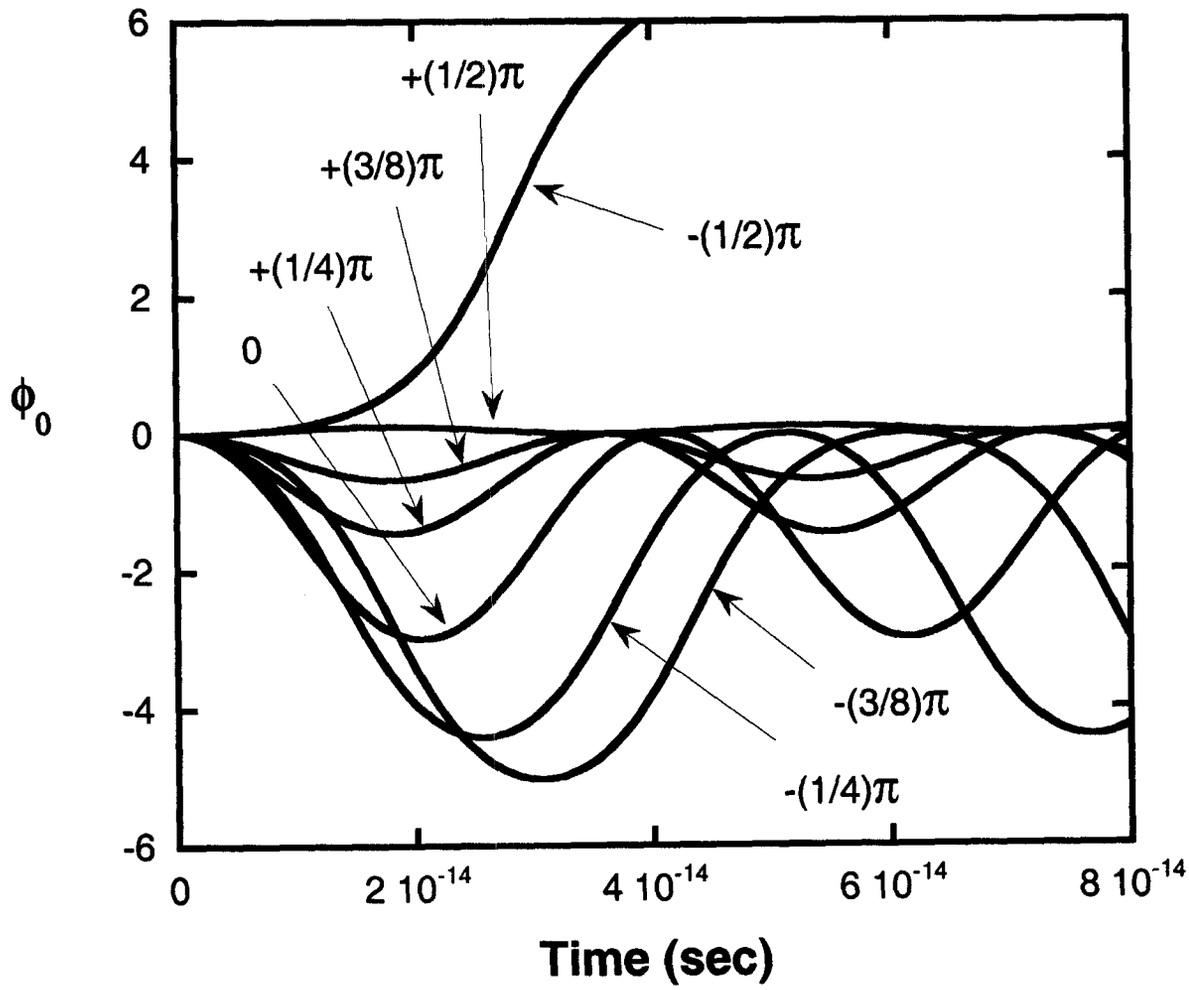
6
4
2
0
-2
-4
-6
ϕ_0
+(1/2)π
+(3/8)π
+(1/4)π
0
-(1/2)π
-(3/8)π
-(1/4)π
0
2 10^-14
4 10^-14
6 10^-14
8 10^-14
Time (sec)

Fig. 7(a)

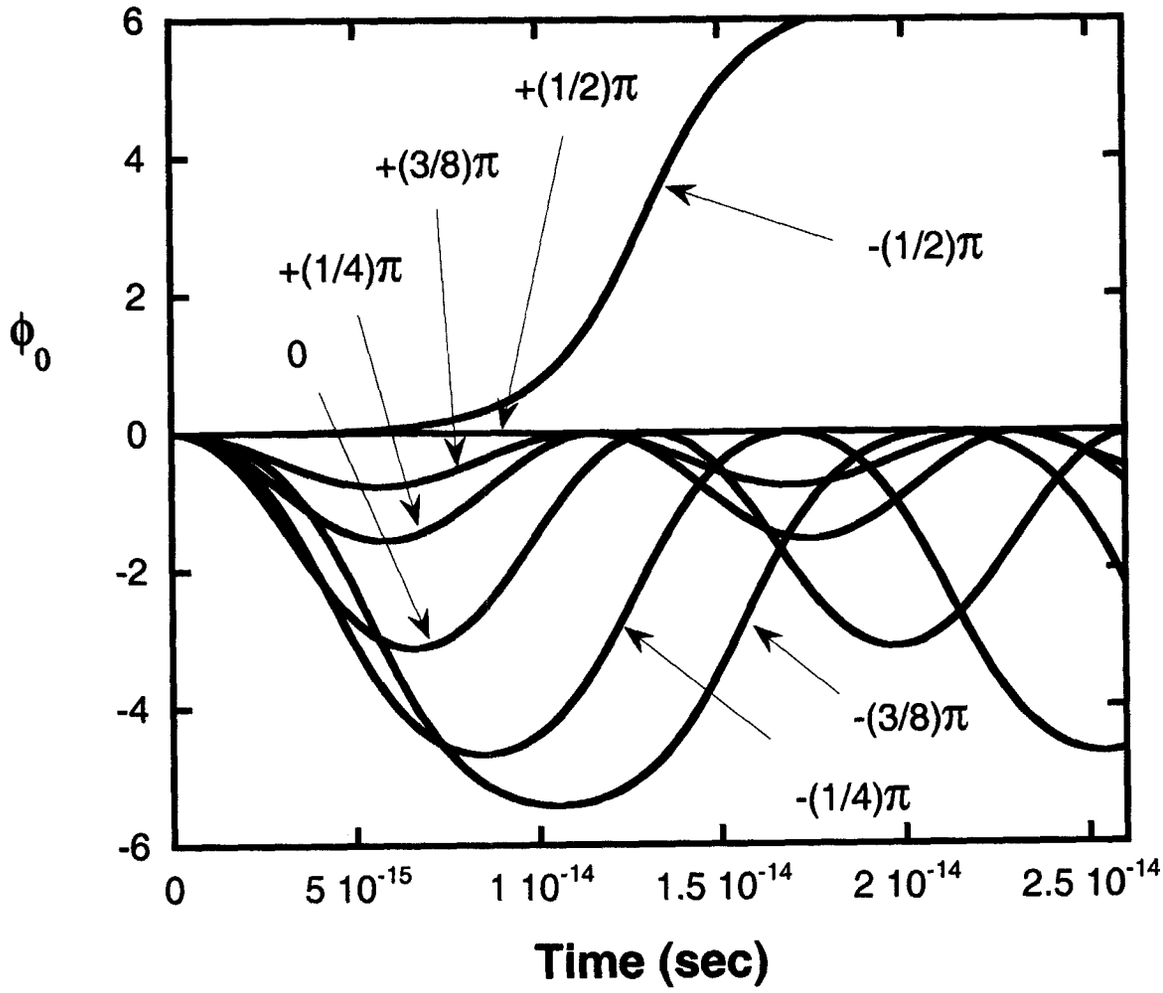
6
4
2
0
-2
-4
-6
ϕ_0
+(1/2)π
+(3/8)π
+(1/4)π
0
-(1/2)π
-(3/8)π
-(1/4)π
0
5 10^-15
1 10^-14
1.5 10^-14
2 10^-14
2.5 10^-14
Time (sec)

Fig. 7(b)

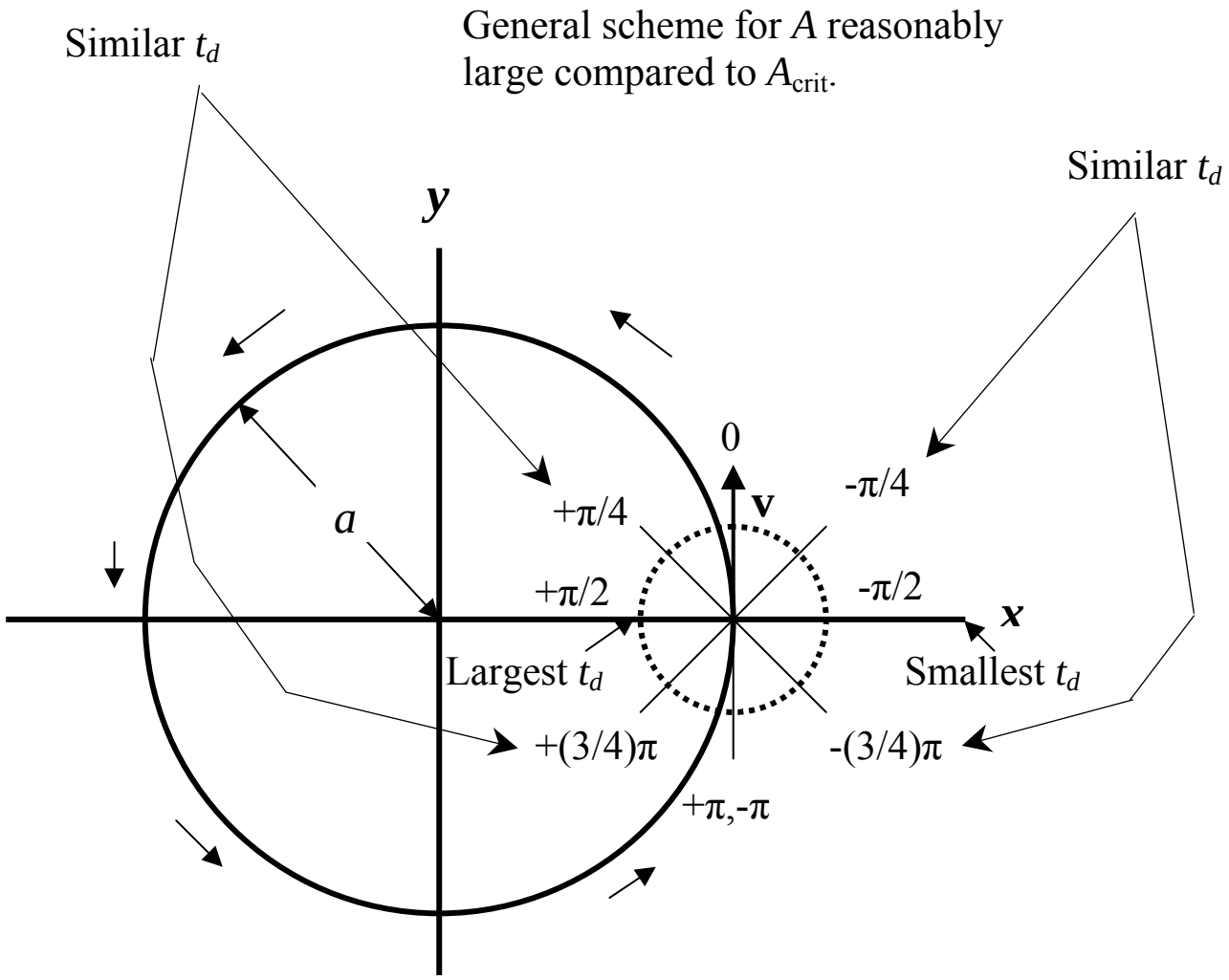
General scheme for A reasonably large compared to A_{crit}.
Similar t_d
Similar t_d
y
x
v
a
0
+π/4
-π/4
+π/2
-π/2
Largest t_d
Smallest t_d
+(3/4)π
-(3/4)π
+π,-π

Fig. 8(a)

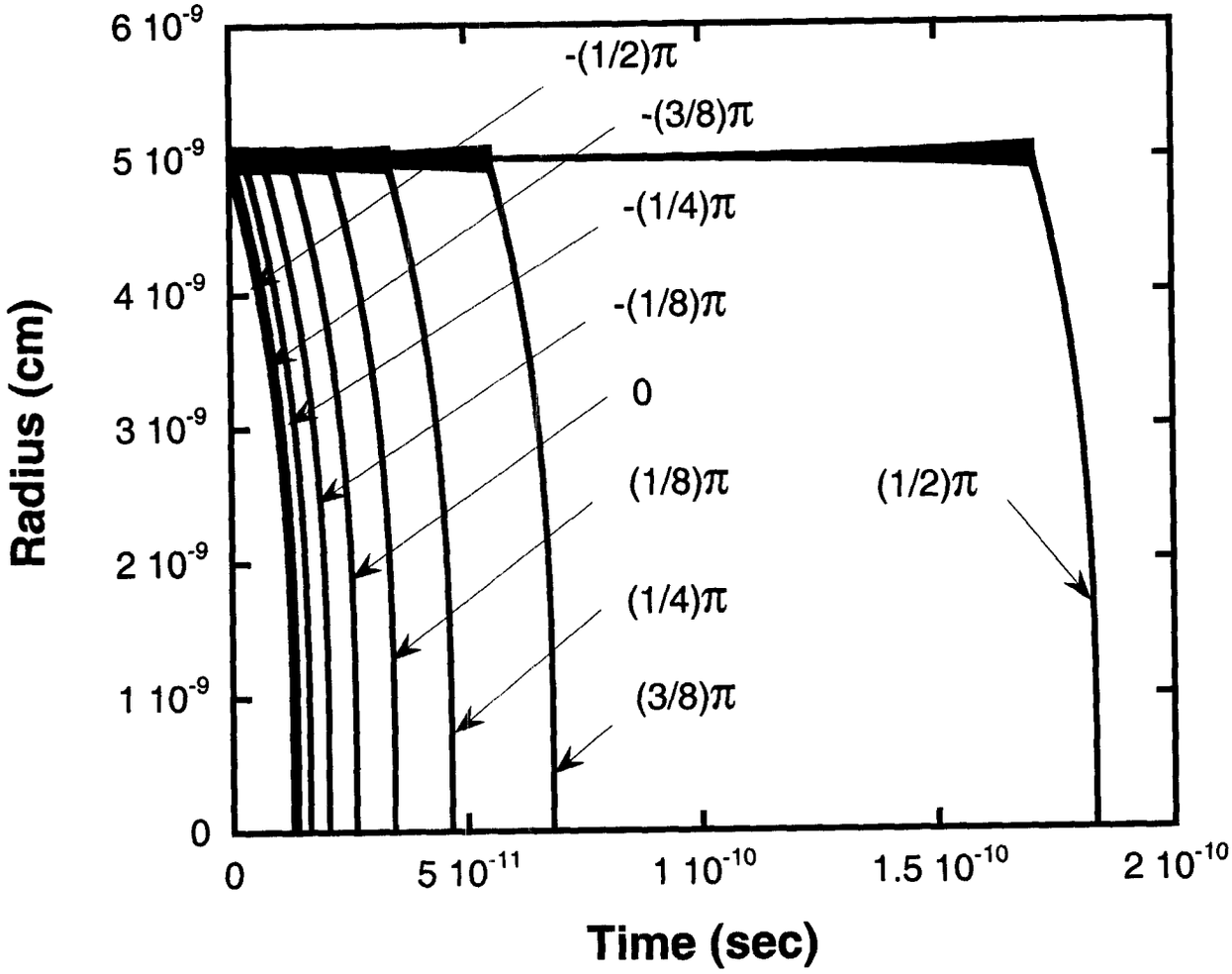
6 10-9
5 10-9
4 10-9
3 10-9
2 10-9
1 10-9
0
Radius (cm)
-(1/2)π
-(3/8)π
-(1/4)π
-(1/8)π
0
(1/8)π
(1/4)π
(3/8)π
(1/2)π
0
5 10-11
1 10-10
1.5 10-10
2 10-10
Time (sec)

Fig. 8(b)

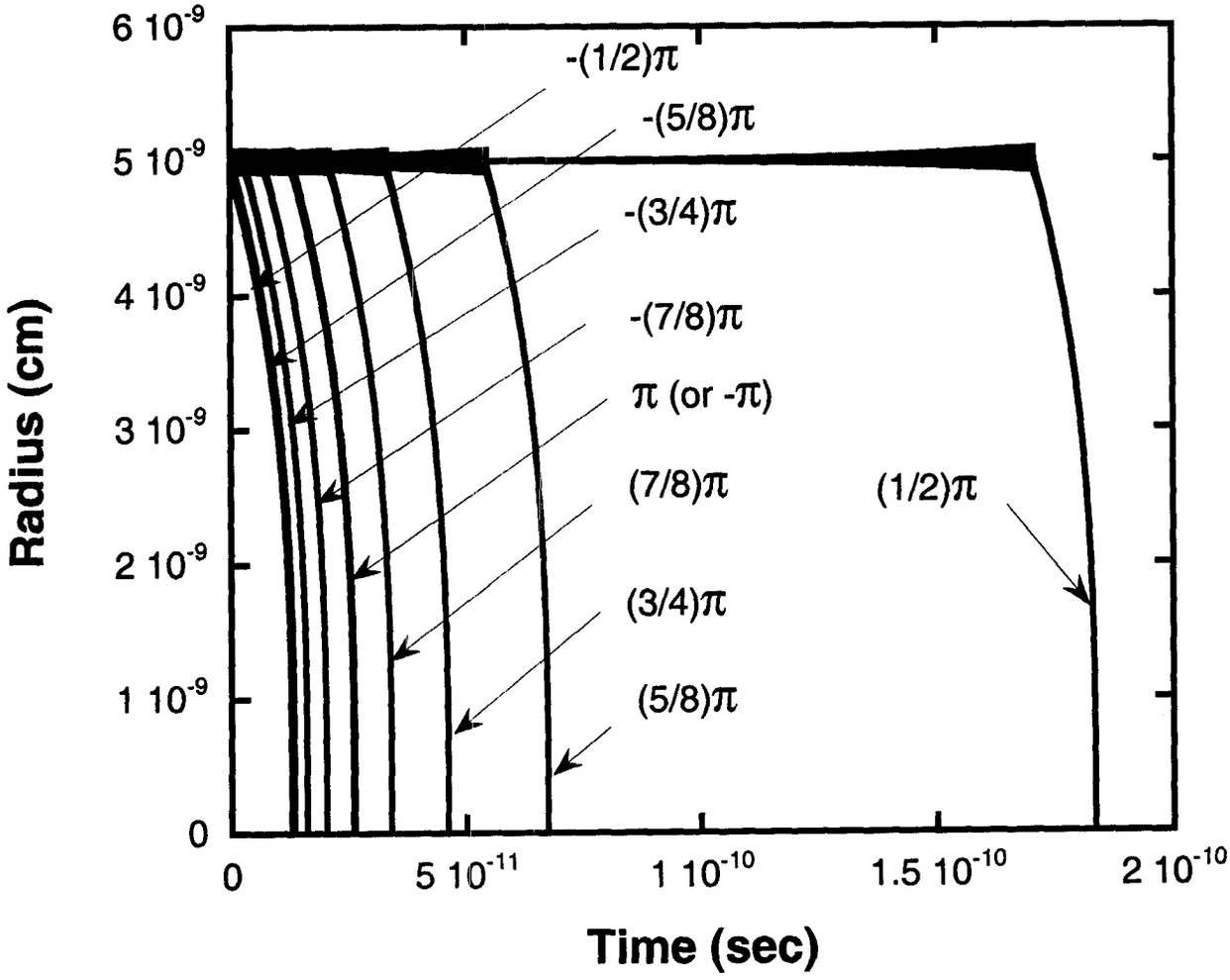
6 10-9
5 10-9
4 10-9
3 10-9
2 10-9
1 10-9
0
Radius (cm)
-(1/2)π
-(5/8)π
-(3/4)π
-(7/8)π
π (or -π)
(7/8)π
(3/4)π
(5/8)π
(1/2)π
0
5 10-11
1 10-10
1.5 10-10
2 10-10
Time (sec)

Fig. 8(c)

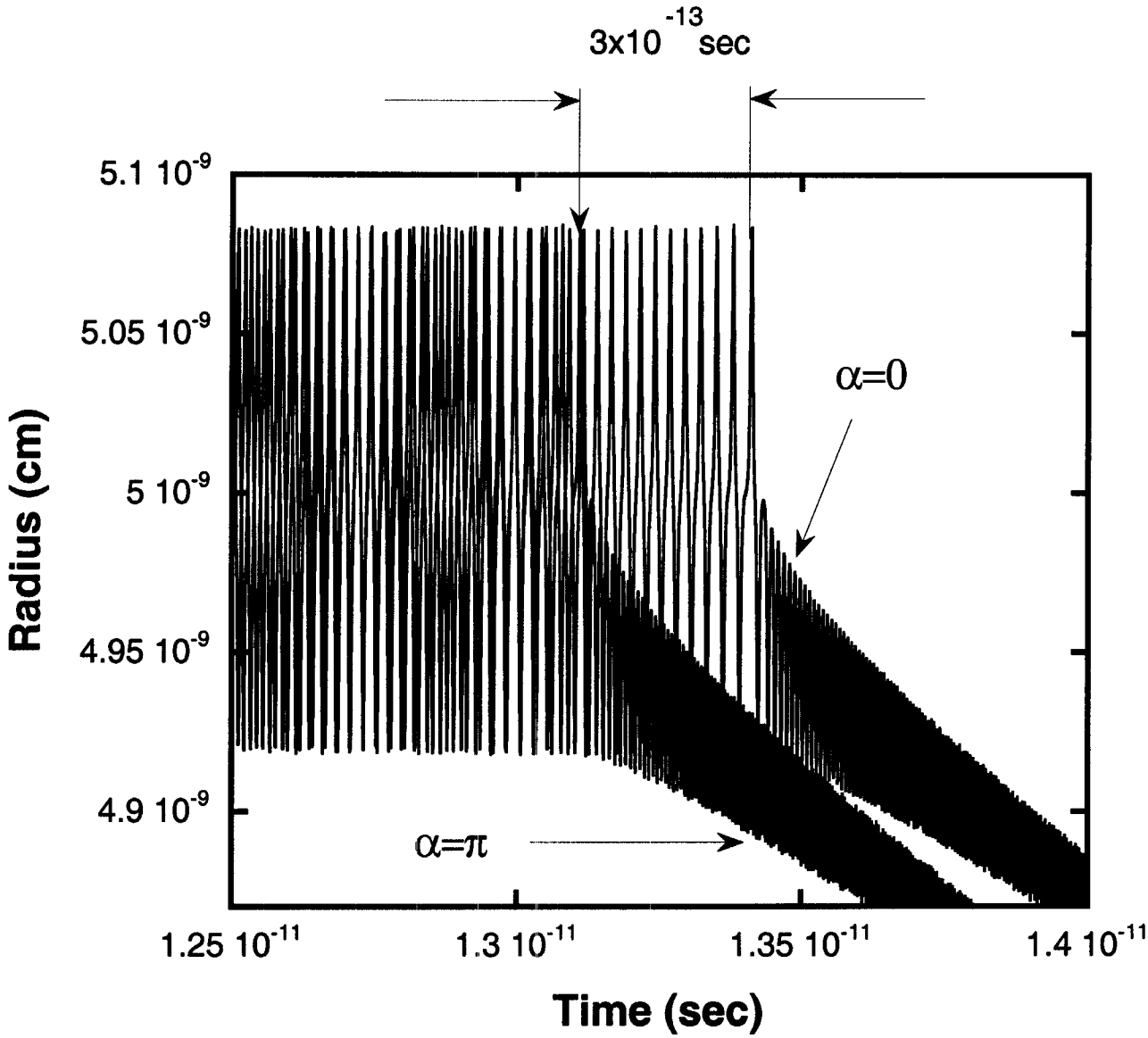
3x10 -13 sec
5.1 10-9
5.05 10-9
5 10-9
4.95 10-9
4.9 10-9
Radius (cm)
α=0
α=π
1.25 10-11
1.3 10-11
1.35 10-11
1.4 10-11
Time (sec)

Fig. 8(d)

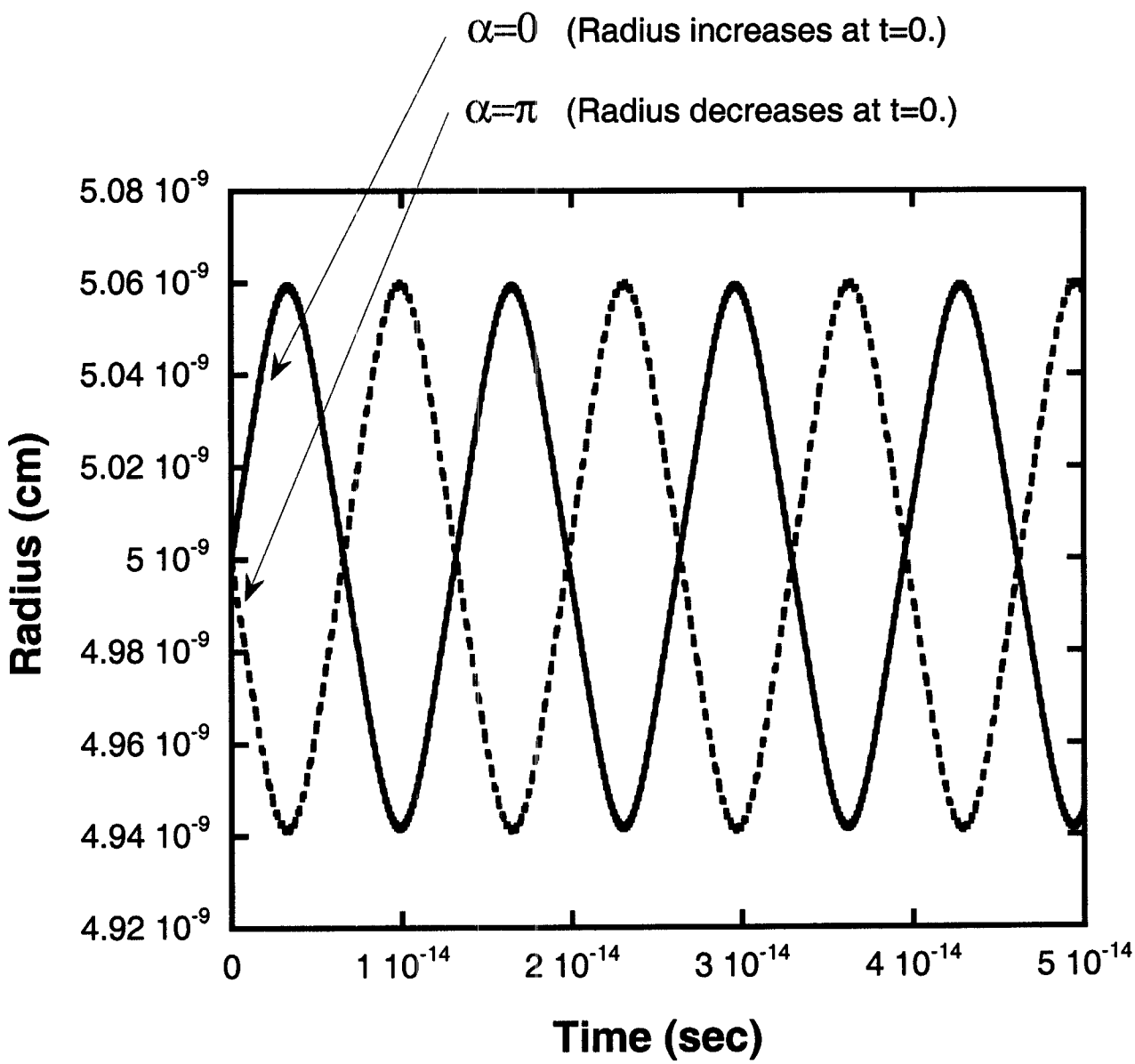
α=0 (Radius increases at t=0.)
α=π (Radius decreases at t=0.)
5.08 10-9
5.06 10-9
5.04 10-9
5.02 10-9
5 10-9
4.98 10-9
4.96 10-9
4.94 10-9
4.92 10-9
Radius (cm)
0
1 10-14
2 10-14
3 10-14
4 10-14
5 10-14
Time (sec)

Fig. 8(e)

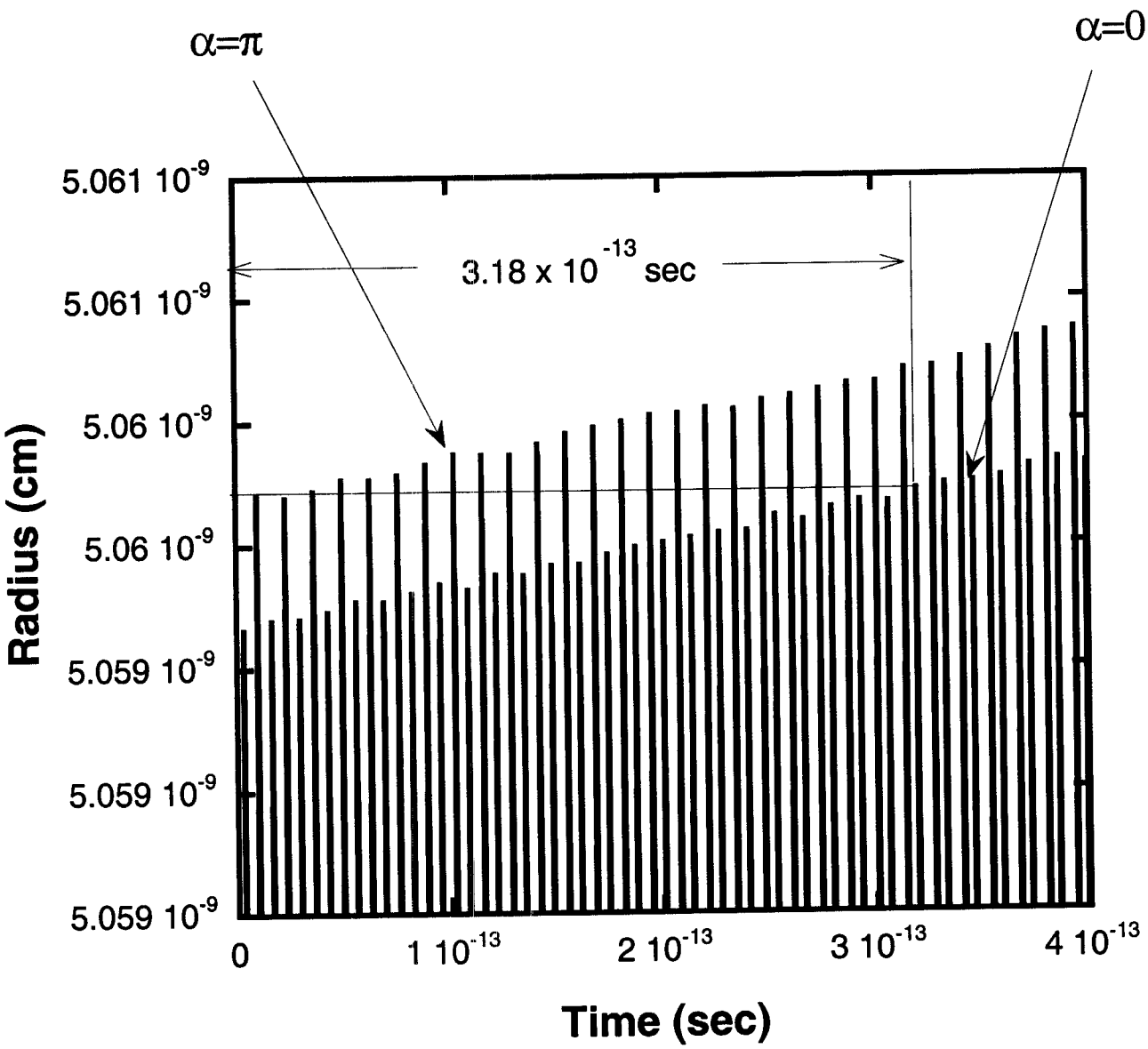
α=π
α=0
5.061 10-9
5.061 10-9
5.06 10-9
5.06 10-9
5.059 10-9
5.059 10-9
5.059 10-9
3.18 x 10-13 sec
Radius (cm)
0
1 10-13
2 10-13
3 10-13
4 10-13
Time (sec)

Fig. 8(f)

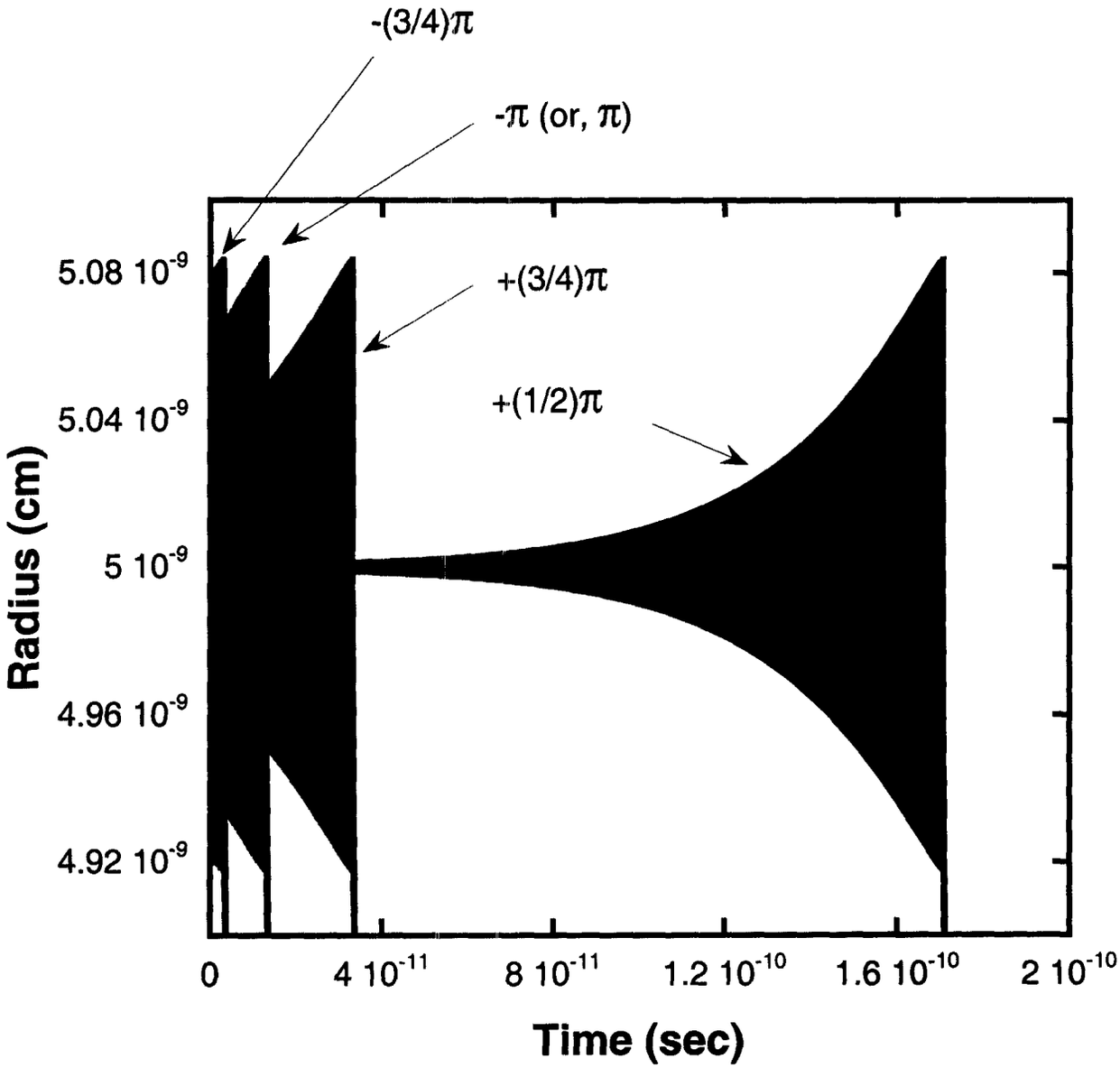
-(3/4)π
-π (or, π)
+(3/4)π
+(1/2)π
5.08 10-9
5.04 10-9
5 10-9
4.96 10-9
4.92 10-9
Radius (cm)
0
4 10-11
8 10-11
1.2 10-10
1.6 10-10
2 10-10
Time (sec)

Fig. 8(g)

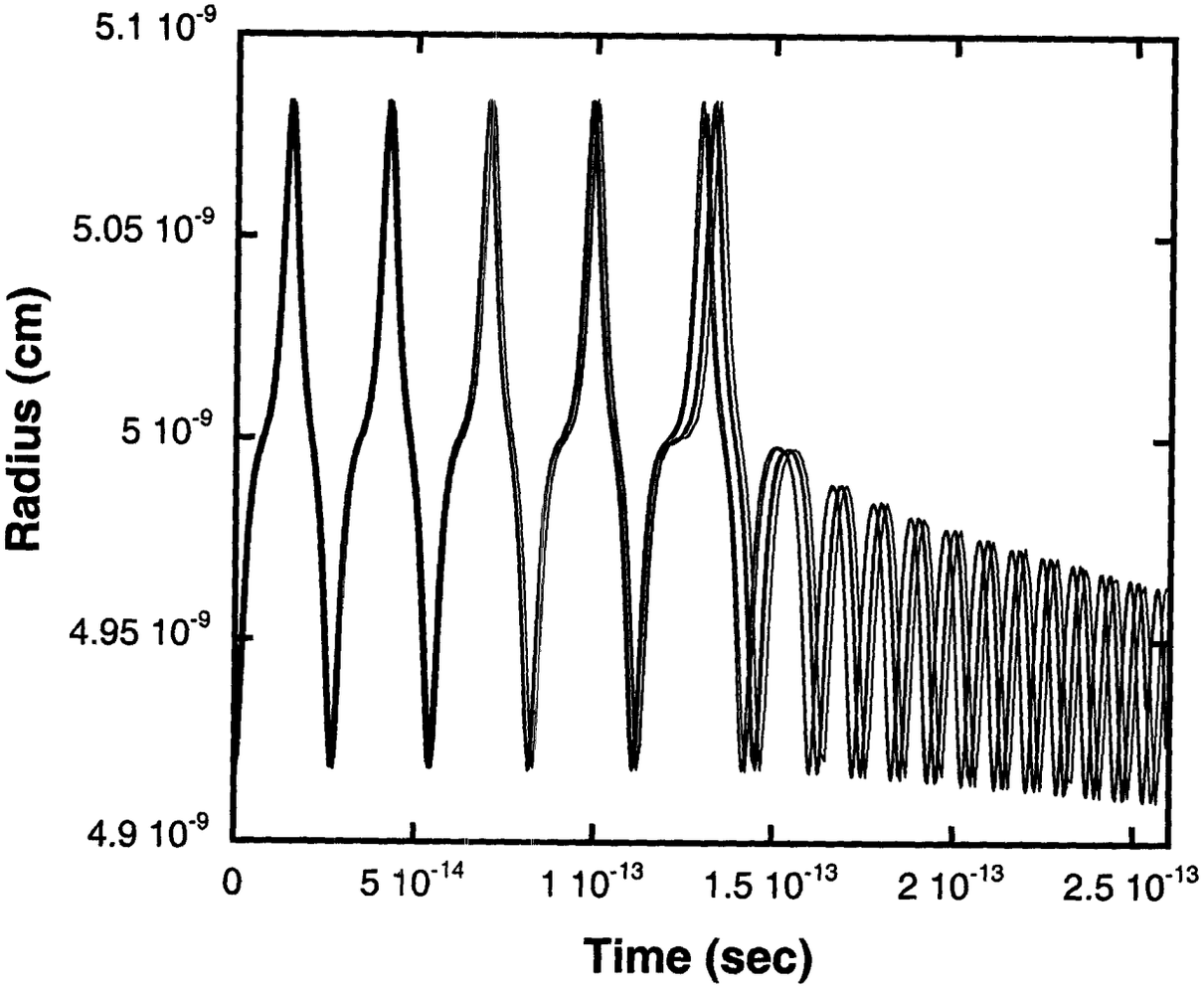
5.1 10-9
5.05 10-9
5 10-9
4.95 10-9
4.9 10-9
Radius (cm)
0
5 10-14
1 10-13
1.5 10-13
2 10-13
2.5 10-13
Time (sec)

Fig. 8(h)

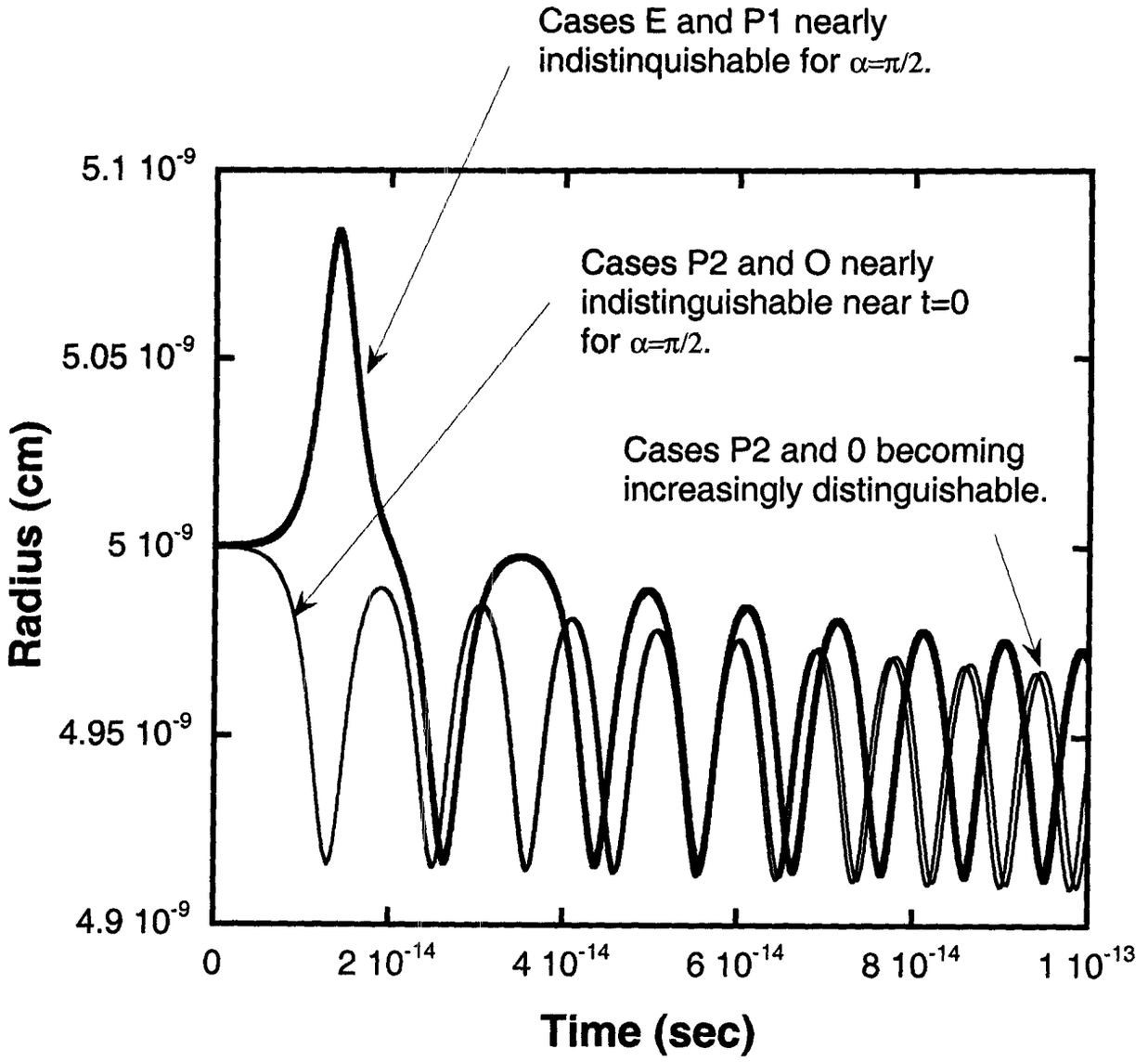
Cases E and P1 nearly indistinquishable for α=π/2.
Cases P2 and O nearly indistinguishable near t=0 for α=π/2.
Cases P2 and 0 becoming increasingly distinguishable.
5.1 10-9
5.05 10-9
5 10-9
4.95 10-9
4.9 10-9
Radius (cm)
0
2 10-14
4 10-14
6 10-14
8 10-14
1 10-13
Time (sec)

Fig. 9